Chair of Petroleum and Geothermal Energy Recovery

Master's Thesis

Analysis of Unstable Flow in Oil-and-Gas Flowline under Carbon Dioxide Corrosion Conditions

Kirill Dubovik

September 2022

MONTANUNIVERSITÄT LEOBEN
www.unileoben.ac.at

AFFIDAVIT

I declare on oath that I wrote this thesis independently, did not use other than the specified sources and aids, and did not otherwise use any unauthorized aids.

I declare that I have read, understood, and complied with the guidelines of the senate of the Montanuniversität Leoben for "Good Scientific Practice".

Furthermore, I declare that the electronic and printed version of the submitted thesis are identical, both, formally and with regard to content.

Date 08.09.2022

Signature Author
Kirill Dubovik

I dedicate my Master Thesis to my family,

who supported me all the time.

Acknowledgements

I express my deep gratitude to my supervisor Alexander Kolchin – Associate Professor of the Department of Transportation and Storage of Oil and Gas in Ufa State Petroleum Technological University, Dipl.-Ing., MBA, Ph.D. in Engineering, for his responsiveness, willingness to help with any difficulties, very clear explanations and friendly communication.

I am also very grateful to Natalya Gulina – Engineer of the Department of Transportation and Storage of Oil and Gas in Ufa State Petroleum Technological University for her contribution to my analysis on corrosion inhibitors, useful tips and assistance in conducting of experiments.

I also express my acknowledgement to Ramzy Albishini – Lecturer of the Chair of Petroleum and Geothermal Energy Recovery in Montanuniversität Leoben, Dipl.-Ing., for his informative instructions, valuable advices and assistance.

Abstract

The main purpose of the study is the mathematical and hydrodynamic analysis of unstable flow in oil-and-gas flowlines under conditions of carbon dioxide corrosion. First of all, the analysis of existing mathematical models describing multiphase flows was conducted. Then, Multiflash was used to create a fluid model, OLGA was implemented for hydrodynamic analysis of the flow, PIPESIM provided an ability of corrosion rate calculation. However, laboratory studies of corrosion inhibitors were done and made it possible to compare experimentally calculated corrosion rates with field test data. It was approved that significant content of carbon dioxide in fluid composition and high water cut magnitudes are the main factors causing corrosion in the considered isolated system. Moreover, the effectiveness of each inhibitor was determined experimentally. In addition, possible ways to solve the pipeline corrosion problem were suggested.

Zusammenfassung

Der Hauptzweck der Studie ist die mathematische und hydrodynamische Analyse instabiler Strömungen in Öl-und-Gaspiplines unter Bedingungen der Kohlendioxidkorrosion. Zunächst erfolgte die Analyse bestehender mathematischer Modelle zur Beschreibung von Mehrphasenströmungen. Dann wurde Multiflash verwendet, um ein Fluidmodell zu erstellen, OLGA wurde für die hydrodynamische Analyse der Strömung implementiert, PIPESIM bot eine Möglichkeit zur Berechnung der Korrosionsrate. Es wurden jedoch Laborstudien zu Korrosionsinhibitoren durchgeführt, die es ermöglichten, experimentell berechnete Korrosionsraten mit Feldtestdaten zu vergleichen. Es wurde bestätigt, dass ein erheblicher Kohlendioxidgehalt in der Fluidzusammensetzung und hohe Wasseranteile die Hauptfaktoren sind, die Korrosion in dem betrachteten isolierten System verursachen. Darüber hinaus wurde die Wirksamkeit jedes Inhibitors experimentell bestimmt. Darüber hinaus wurden mögliche Wege zur Lösung des Problems der Rohrleitungskorrosion vorgeschlagen.

Table of Contents

Chapter 1

Introduction

1.1 Background and Context

By the 21st century, oil production, transportation, treatment and refining technologies have become the most advanced. The use of resource-saving technologies, composite materials and information technologies helped to bring the oil industry to a new, more advanced level. But still, at the moment, most oil companies are faced with the acute issue of minimizing the likelihood of accidents and emergencies, which occur due to unusual properties of oil-and-gas mixtures extracted from oil-bearing horizons.

Often, oil-and-gas mixtures extracted from production wells, enters the oil-and-gas flowline. Properties of oil-and-gas mixtures vary over a wide range and depend on a large number of factors, such as lithologic and facies, geological, physics, chemicals and hydrodynamics. However, methods of oil and gas extraction play important role too. A particular emphasis should be given to the pipeline transport system, the main task of which is the transportation of oil-and-gas mixtures extracted from production wells.

In many cases, a flow in oil-and-gas flowlines is characterized as unstable. The presence of undesirable impurities in oil-and-gas mixtures, such as hydrates, soild particles, CO_2, H_2S, further aggravates the situation. This leads to various accidents and emergencies.

The presence of CO_2 in oil-and-gas mixtures reduces viscosity, simplifying the processes of production and transportation. But at the same time, CO_2 causes corrosion of oil and gas equipment. That is why there is an urgent need to analyze unstable flows in oil-and-gas flowlines under conditions of carbon dioxide corrosion.

1.2 Scope and Objectives

The purpose of the Master Thesis is the mathematical and hydrodynamic analysis of unstable flow in oil-and-gas flowlines under conditions of carbon dioxide corrosion.

To achieve this, the following objectives were set:

- analysis of existing mathematical models describing multiphase flows;

- analysis and modeling of processes occurring in unstable flow in oil-and-gas flowline under conditions of carbon dioxide corrosion;

- laboratory studies of corrosion inhibitors and determination of their effectiveness.

1.3 Achievements

The Thesis considers and mathematically substantiates the unstable flow in an isolated system, which is the oil-and-gas flowline, under conditions of carbon dioxide corrosion. Also, laboratory studies of corrosion inhibitors were carried out on various reservoir water models with determination of their effectiveness. The knowledge obtained can be used in field conditions.

1.4 Technical Issues

No such mathematical or physical model was found that would fully and in detail describe unstable flow in oil-and-gas flowlines under conditions of carbon dioxide corrosion.

Chapter 2

Literature review

2.1 Models of multiphase liquid-solid two-phase flow

Physical phases of matter consist of vapour, liquid, and solid of various crystalline forms. Multiple interactions occur at the interfaces of various configurations or geometries in a flow system with a mixture of phases. Multiphase flow contains a multiplicity of elements of different dynamic responses. For instance, a gaseous suspension of solid particles of identical material can be considered. In multiphase flow, particles of different sizes constitute different phases because of their different inertial responses to a changing flow field (Soo, 1989).

Similar cases may be described in terms of bubbles, droplets and particles suspended in a fluid (gas or liquid), as long as phases are immiscible. Generally, these phases can be separated by various configurations of interfaces. The dynamics of multiphase systems include mass, momentum, energy and charge transfers between phases, whether or not they are in the presence of a potential field. There are some examples of multiphase systems among engineering equipment and processes:

- gas-solid particle systems: gas pipelines, fluidized beds, dust collectors, pneumatic conveyors, heterogeneous reactors, cosmic dusts;
- gas-liquid droplet systems: dryers, absorbers, combustors, atomizers, scrubbers, cryogenic pumping, gas cooling, evaporation;
- liquid-gas bubble systems: air lift pumps, absorbers, evaporators, scrubbers, flotation, aeration cavitation;
- liquid-gas systems: surface waves of air over water, boiling and nuclear reactor safety;
- liquid-liquid systems: emulsifying, extraction, homogenizing;
- liquid-solid particle systems: oil flowlines, sedimentation, flotation (Soo, 1989).

In general, solid particles are non-spherical but isometric. On the contrary, small liquid droplets attain a spherical shape due to surface tension. When gravity or other field forces are significant, these droplets attain smallest flow resistance shapes, such as falling rain droplets. In addition, gas bubbles retain spherical shape due to surface tension until modified by field forces (Soo, 1989).

2.1.1 Single-particle dynamic model

Researches on the theory of liquid-solid two-phase flow began in the 1940s (Tchen, 1947). Single-particle dynamic model first appeared. The model states that solid particles have independent, stable and regular movement in flow field meaning that they have no effect on flow pattern. A very significant thing is that interphase interaction is not considered in this model.

2.1.2 The PSI-CELL model

The capability to predict changes of temperature and velocity of a cloud of droplets suspended in a gas flow is essential in the design of many industrial processes. The main problem in analyzing a two-phase flow (gas-droplet flow) suspension lies in defining the coupling of mass, momentum and energy between phases. These coupling phenomena include very complex interactions that affect both gas and droplet phases (Figure 2.1).

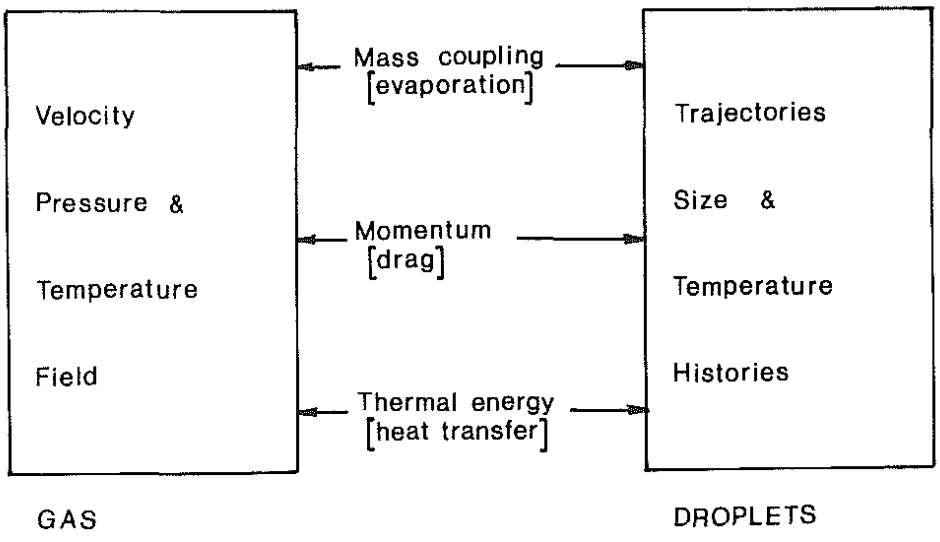

Figure 2.1: Gas-droplet coupling phenomena

It has to be mentioned that interphase interaction is not considered in the single-particle dynamic model (Tchen, 1947). The Particle-Source-In Cell (PSI-CELL) model for gas-droplet flows or particle trajectory model was proposed in 1977 (Crowe, Sharma & Stock, 1977). It is based on the research result of gas-droplet two-phase flow. This model improves the single-

particle dynamic model (Tchen, 1947) by taking liquid-solid interaction into account using hydrodynamic equation. The following aspect takes the model closer to flow reality of two-phase flow. Single-particle dynamic model and the PSI-CELL model propose a fluid as a continuous media and a particle as a discrete media respectively.

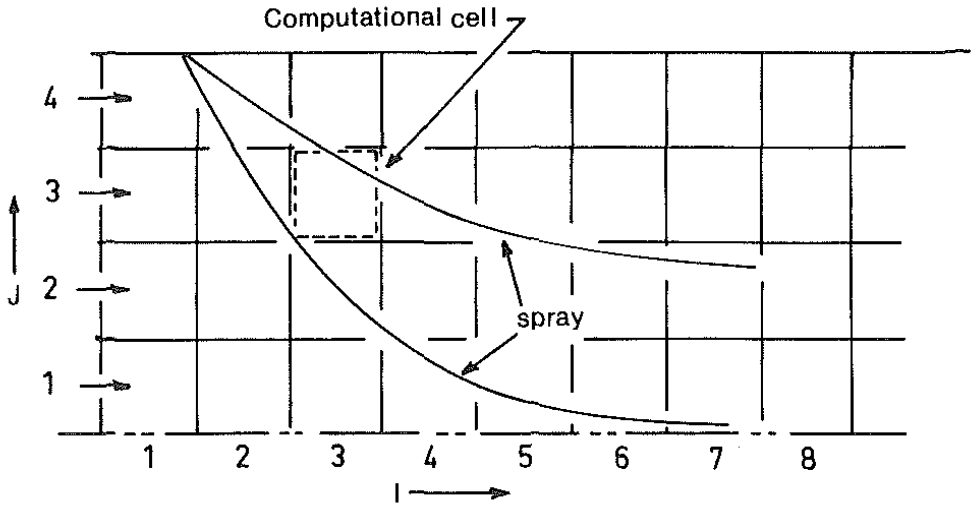

Figure 2.2: Illustrative cell structure used in PSI-CELL model

The main peculiarity of the PSI-CELL model is a necessity to subdivide the flow field into a series of cells, as shown in Figure 2.2. The example shown in Figure 2.2 is a spray issuing into a moving gas stream and each cell is regarded as a control volume for the gaseous phase. As droplets traverse a given cell in the flow field they may be:

- evaporating or condensing, resulting in a source (or sink) of gaseous mass to the fluid in the cell;
- accelerating or decelerating, resulting in a momentum augmentation or deficiency in the fluid in the cell in the direction of droplet motion;
- conducting heat or convecting enthalpy, resulting in a source (or sink) of thermal energy to the fluid in the cell (Crowe, Sharma & Stock, 1977).

For each cell, finite differential equations for mass, momentum and energy conservation are used. The continuum flow field is then analyzed. By solving the system of differential equations constituting the finite differential equations for each cell, the entire flow-field solution is achieved. By integrating the equations of motion for droplets in the gas flow field, the droplet trajectories, size and temperature history are obtained. Then, equations are solved for the droplet velocity, size and temperature along particle trajectories. The droplet source terms for the gas flow equations are provided by recording the mass, momentum and energy of the droplets on crossing cell boundaries.

The complete solution for a gas-droplet flow field is illustrated in Figure 2.3. The calculation is started by solving the gas flow field with assumption that no droplets are present. Having this flow field, droplet trajectories with size and temperature histories along the trajectories are calculated. Then, throughout the flow field, the mass, momentum and energy source terms for each cell are determined. Incorporating these source terms, the gas flow field is solved again. The new gas flow field is used for establishing new droplet trajectories and temperature histories, which constitute the effect of the gas phase on the droplets. When several iterations are done, the flow field equations are satisfied to a predetermined value. Consequently, this is how to obtain the solution, which accounts for the mutual interaction of the droplets and gas.

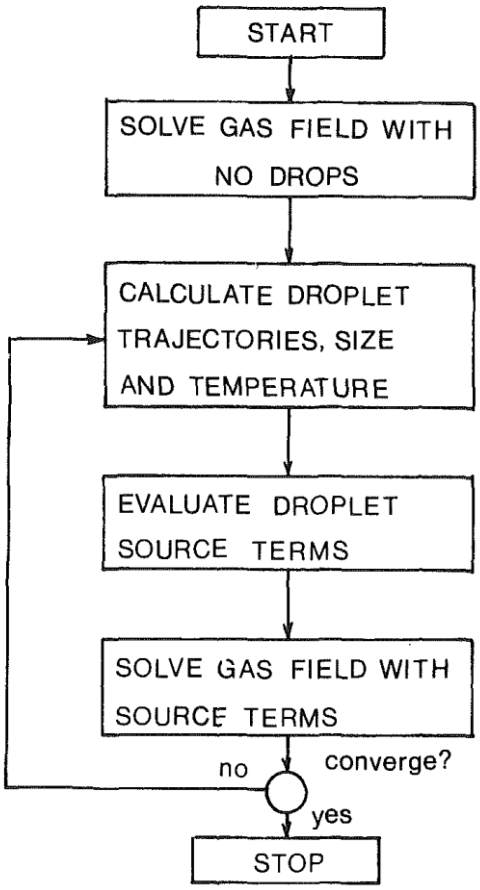

Figure 2.3: Flow chart for PSI-CELL computational scheme

All in all, the PSI-CELL model provides possibilities of incorporating the complex coupling phenomena in multiphase flows into a calculation scheme by regarding the droplets as sources of mass, momentum and energy. In general, the model is a reliable framework for different two-dimensional multiphase flow problems analysis. However, the PSI-CELL model is equally applicable to problems in heterogeneous combustion, such as droplet or coal-particle burning.

2.1.3 Dispersion model

Soo introduced a dispersion model in his book (Soo, 1989). The main idea of this work is that discrete particles are represented as continuous media (pseudo-fluid). It is also important that Soo used the continuous medium theory to study and describe movement of granular media. In addition, the author considered the turbulent diffusion processes between fluid and particle phase.

2.1.4 Single fluid model

Problems of two-dimensional and three-dimensional steady flows calculations in combustion systems were observed by Spalding (Spalding, 1972). A combustion system is a stream of gaseous and solid phases, which is then partially mixed with air. Solid particles and soot in flames may be of fuel or of combustion products. The author came up with a new model to calculate processes in a combustor. Single fluid model holds that the particle phase should satisfy the continuity equation only and no relative motion between solid particles and fluid exists.

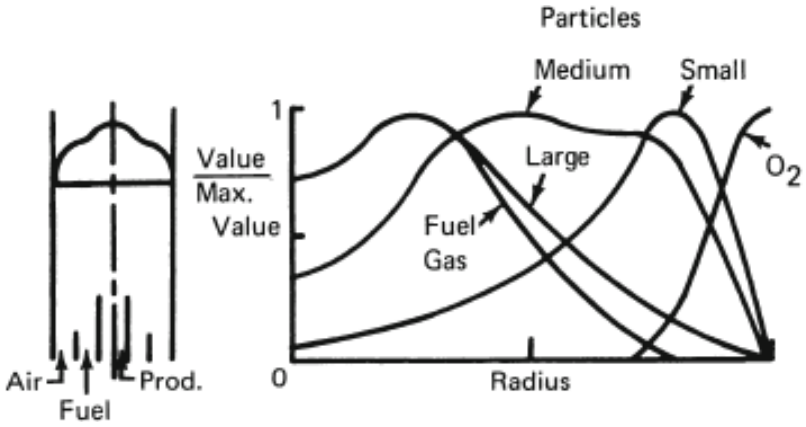

Figure 2.4: Results of computation for injection of large fuel particles in the fuel-gas stream

Figure 2.4 represents the results of calculations for a particular combustion system in which a stream of gaseous and solid fuel, after partially mixing with an annular stream of air, is ignited by a stream of hot combustion products. The left-hand diagram shows the system, while the right-hand one illustrates the computed profiles of fuel and oxygen near the downstream end of the duct.

The concentration profiles of gaseous fuel and oxygen are typical for diffusion flames. The general attention should be paid to curves for small, medium and large particles. Small particles have their highest concentration in the oxygen-rich region and the profile has similarities to the oxygen's one. While, by contrast, profile for large particles resembles to that for gaseous fuel, but it extends farther into the oxygen-rich region.

2.1.5 Liquid-solid two-phase flow model

Bowen was studying thermodynamics of mixtures to describe incompressible porous media models (Bowen, 1980). An incompressible porous material is a mixture where the solid matrix and each pore fluid are both incompressible. The assumption of incompressibility implies a certain constraint among the variables. Thus, he applied classical theories of gas mixtures to porous media modeling. Also, he discussed the flow of immiscible fluids in deformable and rigid solid matrices.

As the single fluid model by Spalding is too simplified, Bowen introduced the liquid-solid two-phase model or so-called 'two-fluid model' in 1980. Consequently, his model considers the turbulent diffusion of each phase. Moreover, interaction between solid particles and interaction between solid particles and fluid are taken into consideration. In addition, Bowen's model also applies a spatial continuous distribution function to describe kinetic and thermodynamic parameters of particle phase.

The liquid-solid two-phase flow model is widely used in oil and gas industry. It is generally involved in the study of sulfur deposition (Pack, Parks & Chesnoy, 2012) wax deposition (Leporini, Terenzi, Marchetti et al., 2019) and hydrate transportation (Song, Li, Wang et al., 2018). But this extraordinary model has its limitations too. The main issue is the unavailability to observe changes to the development of solid particles during production processes.

2.1.6 Particle population balance model (PBM)

Basically, the first-ever population balance model was proposed by Smoluchowski in 1917 (Wang, Yu & Peng, 2019). It is a coagulation equation describing the time evolution of the number density of particles as they coagulate to a particular size at particular time and is also suitable for hydrate particles transportation (Song, Li, Wang et al., 2018). This model supposes that particles are mainly controlled by Brownian action, laminar flow and turbulence.

The liquid-solid two-phase flow model (Bowen, 1980) mainly depicts the impact of interaction between a liquid-phase solvent and a solid-phase solute on the flow field during the flow process. Unfortunately, it is impossible to consider changes to the development of solid particles via application of this model. Thus, a kind of advanced version of liquid-solid two-phase flow model had to be created. According to the law of conservation of particle mass, the particle population balance model (PBM) was proposed by Hulburt & Katz (Hulburt & Katz, 1964). This model describes the growth and change to solid particles. A very unusual fact that it was invented 16 years before the liquid-soild two-phase flow model (Bowen, 1980).

An engineering analysis requires the dependence of particle nucleation and growth on the particle environment. Then, this data is incorporated into differential equations in order to

observe how such quantities as average particle size vary with position in the processing unit. These differential equations can be used correspondingly with an overall set of differential equations viewed as a mathematical characterization of the processing system (Hulburt & Katz, 1964).

Hulburt & Katz established a phase space for a typical particle, whose coordinates specify the location of the particle as well as its quality. Equations of motion, in the form of ordinary differential equations showing how these phase coordinates evolve in time. Moreover, the equations of motion reflect the influence of the hydraulic and chemical environment of the particle. A partial differential equation for the number density of particles in the phase space is developed from the equations of motion. This equation is an analogue of the classical Liouville equation that expresses the conservation of probability in the phase space of a mechanical system. The combination of this modified Liouville equation, regular transport equations and suitable initial and boundary conditions is a complete mathematical characterization of the system being studied (Hulburt & Katz, 1964).

However, this complete system characterization is very sophisticated mathematically and over-detailed for many engineering purposes. It means that much less than a knowledge of the full distribution of particle sizes at every position in the processing unit has to be analyzed. In order to simplify a system under study, Hulburt & Katz recognized significant aspects. Firstly, phase coordinates of a particle can be separated into two parts: a set of external coordinates, which specify the location of the particle in the processing unit, and a set of internal coordinates, which specify the particle size and such other aspects of the particle quality. Secondly, the number density of particles in the phase space can be represented as a distribution over the internal coordinates, with the external coordinates appearing as parameters. All in all, an approximate system description is furnished by the leading moments of this distribution: the average particle count, the average measure of size (or other aspects of quality) of a particle, the variance of particle sizes, etc. All these parameters have to be considered as functions of the external coordinates, that is, of position in the processing unit. Afterwards, the modified Liouville equation can be reduced to differential equations in just these moments, viewed as functions of the external coordinates.

In any case, the resulting differential equations in the moments by Hulburt & Katz have the same dimension of dependence as regular transport equations. Consequently, these two sets of equations may conveniently be joined for mathematical solution. This combined set of equations is a working characterization of transport processes in systems with a particulate phase. In general, the PBM by Hulburt & Katz successfully describes the primary crystallization processes – crystal nucleation and growth in one-dimensional and higher-dimensional systems. In addition, a primitive theory of collisional agglomeration is determined

via application of this model. Moreover, further modified version of PBM can also describe processes devoted to secondary crystallization - crystal coalescence (Wang, Yu & Peng, 2019), (Song, Li, Wang et al., 2018), crystal breakage (Fan, Marchisio & Fox, 2004) and deposition of solid particles (Park & Lee, 2002)

Initially, PBM began to be utilized in chemistry. In chemical applications, PBM provides association of microscopic behavior (nucleation, growth, agglomeration, breakage) of the discrete phase with its macroscopic properties (volume, area, particle size) by means of tracking the quantity density function variation of it. At present, PBM has been widely used in the chemical processes of crystallization, flocculation, polymerization, granulation and multiphase flow (Song, Li, Wang et al., 2018).

2.1.7 ASL growth model

Abegg, Stevens and Larson introduced ASL growth model – the empirical size-dependent growth rate model, which has more advanced properties (Abegg, Stevens & Larson, 1968).

It is well-known that crystal growth consists of three basic steps:

- diffusion of solute molecules from the bulk of the solution to the crystal-solution interface;
- surface reaction as the solute molecules are arranged into the crystal lattice;
- diffusion of the heat of crystallization from the crystal solution interface back into the bulk of the solution.

The effect of the last step on the overall crystal growth rate was not studied extensively when the model was published. However, in most crystallization systems with relatively low heat of crystallization, the effect of the last step on the overall growth process is quite small in comparison with two previous steps.

ASL growth model is capable of fitting data to indicate a growth rate proportional to crystal size. In addition, the model is capable of describing systems where growth rate is inversely proportional to size. This size-dependent model is a commonly used particle growth model. The model can be described by equation (2.1):

$$G(L) = G_0(1 + aL_p)^b \tag{2.1}$$

where G_0 is the growth rate of the crystal nucleus (m/s); L_p is the particle size (m); a and b are model parameters and can be obtained experimentally.

2.1.8 Growth and change model of solid particles in water-injection pipeline

Despite the extensive application studies on the particle population balance model, these studies usually only considered the change to solid particles with time and flowrate and ignored the impact of Brownian diffusion on small solid particles, that are less than 1 μm (Song, Li, Wang et al., 2018). There were no models which could fully reflect the growth and change to small particles affected by Brownian motion in the injected fluid before 2020.

To describe the growth and change to solid particles in the liquid phase pipeline, the method of coupled liquid-solid two-phase flow model (Bowen, 1980) and particle population balance model (Hulburt & Katz, 1964) was invented in 2020 (Li, Li, Wang et al., 2020) Furthermore, such parameters as operating conditions of injected water, test results of particle size and content of solid particles in a certain block of Shengli Oilfield were analyzed too. Finally, the growth and change model of solid particles in water-injection pipeline was established. Here are assumptions to be considered while applying the model:

- operating conditions of injected water should be stable;
- transportation process of injected water is approximated as a steady flow;
- content of solid particles in the injected water is much less than 1 wt% of water mass – the impact of solid particles on liquid phase flow can be neglected;
- the injected water flow can be approximated as a single-phase liquid flow, as shown in Figure 2.5. Also, mass (continuity), momentum, energy conservation equations can be simplified as shown in equations (2.2-2.4) respectively;
- the brine density effect (El-Dessouky & Ettouney, H. 2002) can be neglected during the transportation of injected water – the flow behavior of the injected water can be approximated as an incompressible and stable flow, which is shown in equation (2.5);
- Shukhov's equation is used for temperature drop calculation as Joule-Thomson effect is neglected.

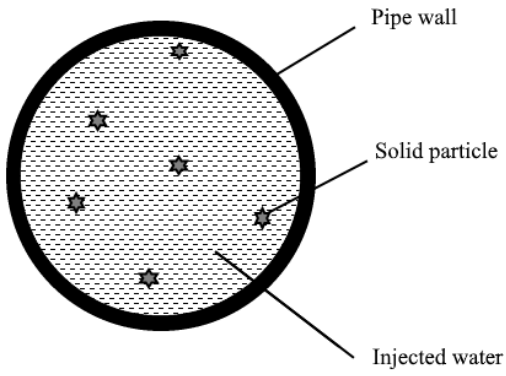

Figure 2.5: Visual representation of the flow process being modeled

All in all, by the simultaneous application of equations (2.2-2.6), the growth and change model of solid particles in water-injection pipeline can be established [10].

Simplified mass (continuity), momentum and energy conservation equations respectively are shown in equations (2.2-2.4):

$$\frac{\mathrm{d}}{\mathrm{d}x}(\rho_l v_l A_l) = 0 \tag{2.2}$$

$$\frac{\mathrm{d}}{\mathrm{d}x}\left(\rho_l v_l^2 A_l\right) = 0 \tag{2.3}$$

$$\frac{\mathrm{d}}{\mathrm{d}x}\left(\rho_l v_l^2 A_l\left(H_l + \frac{v_l^2}{2}\right)\right) = Q_x \tag{2.4}$$

where ρ_l is the density of liquid phase (kg/m^3); v_l is the velocity of liquid phase (m/s); A_l is the parameter of liquid phase, Q_x is the energy transfer source term (J).

If the brine density effect (El-Dessouky & Ettouney, H. 2002) is neglected, the energy conservation equation is shown in equation 2.5:

$$\left(\frac{\partial h}{\partial T}\right)_P \frac{\mathrm{dT}}{\mathrm{d}x} + \left(\frac{\partial \mathrm{h}}{\partial \mathrm{T}}\right)_{\mathrm{T}} \frac{\mathrm{dP}}{\mathrm{dx}} = -\frac{\mathrm{dQ_x}}{\mathrm{dx}} \tag{2.5}$$

where P is the pressure (Pa); T is the temperature (K).

Population balance model proposed by Smoluchowski is shown in equation 2.6 (Wang, Yu & Peng, 2019):

$$\frac{\partial n(v,x,t)}{\partial t} + \nabla\big(Vn(v,x,t)\big) - \nabla\big(D_x \nabla n(v,x,t)\big) = S(v,x,t) \tag{2.6}$$

where $n(v, x, t)$ is the particle number density function (a/m^3); V is the average rate of the v particle in the i direction (m/s); D_x is the diffusion coefficient; $S(v, x, t)$ is the kernel function of dynamic events of particles, such as growth, coalescence, breakage and deposition kernel functions.

The key to solve the growth and change model of solid particles in water-injection pipeline – is the solution to particle population balance equation. The used methodology is Direct Quadrature Method of Moments (DQMoM) (Fan, Marchisio & Fox, 2004). This tool allows to track the overall info on solid particles along the path, such as coalescence amount, particle size, etc, but it is unable to reflect the specific particle size distribution (PSD). For this purpose, the moment-based particle distribution model is utilized to fulfill this task. (Pope, 1980). In general, the model is successfully verified as the average error of the fitting degree of PSD equals 6.9% and the average relative error of median diameter equals 4.1% (Li, Li, Wang et al., 2020).

The growth and change model of solid particles in water-injection pipeline was successfully applied to research different phenomena by taking the water-injected pipeline between the center united station (CUS) and the injection wells as the research object (Li, Li, Wang et al., 2020):

- firstly, the effect of CUS outlet flowrate on PSD of wellheads was examined. It was observed that increased flowrate reduces the coalescence and the effective collision probability between particles, as shown in Figure 2.6. Consequently, it causes a decrease in the particle growth rate. This aspect is consistent with the experimental phenomenon (Ho & Sommerfeld, 2002);

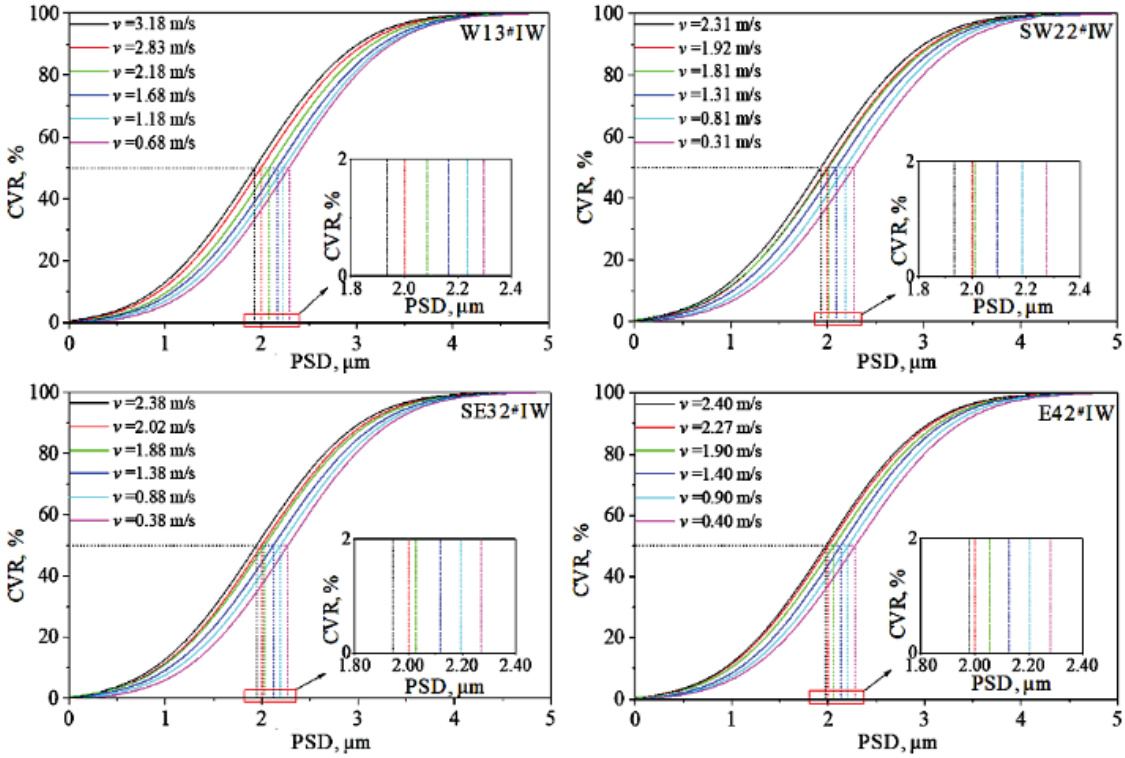

Figure 2.6: Influence of CUS outlet flowrate on PSD of wellheads

- secondly, the influence of CUS outlet temperature on PSD of wellheads was studied. It was defined that increased temperature reduces the effective collision probability between particles (because of excessive kinetic energy). Therefore, the particle growth rate decreases too, as shown in Figure 2.7. This fact also corresponds with the experimental phenomenon (Ho & Sommerfeld, 2002). Moreover, the increased temperature reduces the nucleation rate of solid particles, which leads to a smaller magnitude of the particle number. This information is confirmed theoretically by Arrhenius (Lewis, Seckler, Kramer et al., 2015);
- thirdly, the impact of PSD of CUS outlet on PSD of wellheads was explored. The discovered result is very intuitive - increased PSD leads to higher magnitude of the particle

growth rate, the particle number, the particle coalescence, the particle nucleation rate, etc, as shown in Figure 2.8.

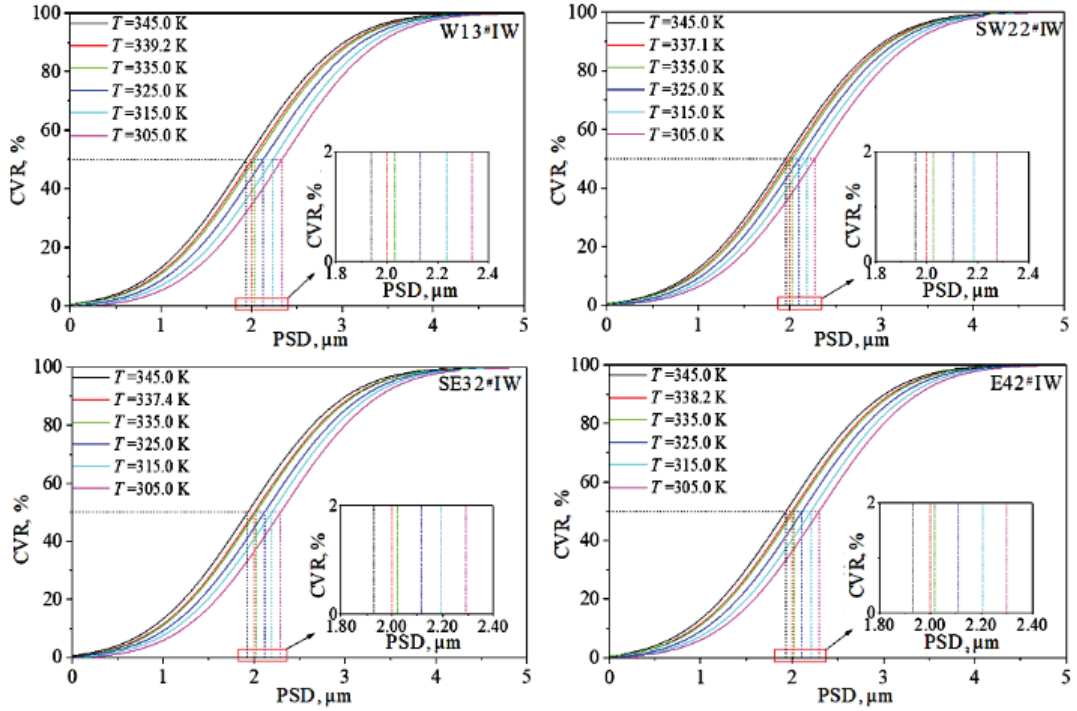

Figure 2.7: Influence of CUS outlet temperature on PSD of wellheads

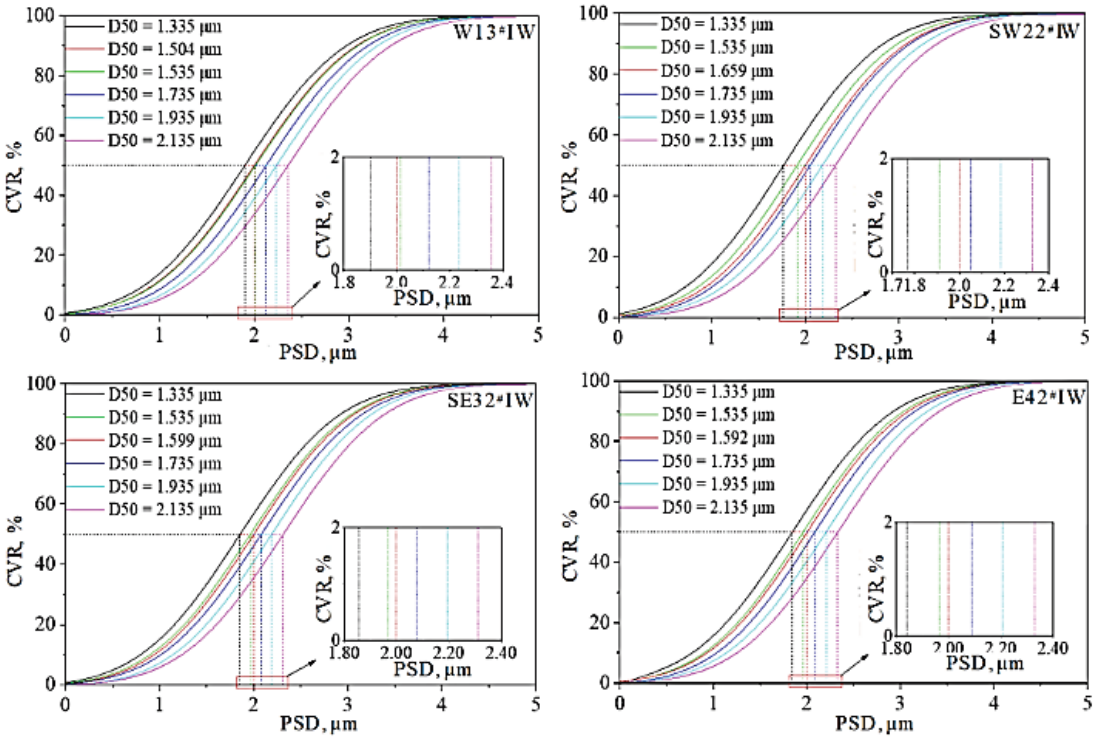

Figure 2.8: Impact of PSD of CUS outlet on PSD of wellheads

As a result, increased flowrate and temperature and reduced PSD allow to meet the control index of the median diameter of solid particle requirements in the injected water, which is less than 2 μm for Shengli Oilfield (Li, Li, Wang et al., 2020).

In general, the model is based on one-dimensional fluid control equation and particle population balance equation. It can be successfully utilized to study the growth and change to solid particles in long-distance water-injection pipeline and to optimize critical magnitudes of flowrate, temperature, PSD on the CUS outlet. Further research on this basis have to define the impact of vertical or inclined pipe section going into and out of the stations and the impact of header section of the water distributing station (WDS).

Chapter 3

Analysis of unstable flow in oil-and-gas flowline

3.1 Statement of the problem

The object of the research is the oil-and-gas flowline from well cluster-7 to OTP 'Chernovskoe'. The flowline is located on the Chernovskoe oilfield in the Udmurt Republic. The oilfield is operated by 'Belkamneft' named after A.A. Volkov, JSC. The flowline consists of five sections, the total length of which is 5370 meters, as shown in Figure 3.1:

- Section 3030 (L = 1250 m) – from the tie-in point of AGMUs of well cluster-7 (valve-46) to the tie-in point of AGMUs of well cluster-2 (valve-39);
- Section 3032 (L = 470 m) – from the tie-in point of AGMUs of well cluster-2 (valve-38) to the tie-in point of flowline Section 3064 (valve-35) and junction point of flowline Section 3065 (valve-33);
- Section 3033 (L = 900 m) – from the tie-in point of flowline Section 3064 (valve-35) to the tie-in point of AGMU of well cluster-16 (valve-30);
- Section 3035 (L = 2250 m) – from the tie-in point of AGMU of well cluster-16 (valve-30) to the tie-in point of AGMUs of well cluster-14;
- Section 3037 (L = 500 m) – from the tie-in point of AGMUs of well cluster-14 to OTP 'Chernovskoe'.

The most significant problem of the oil-and-gas flowline from well cluster-7 to OTP 'Chernovskoe' is oil leaks caused by corrosion. Unfortunately, ruptures occur very frequently, polluting the nature and affecting operational processes of oil and gas production and transportation. Point locations of ruptures and pipe leaks occurred from January 2021 to August 2021 are shown in Figure 3.1.

More detailed data on Sections 3033 and 3035 is shown in Table 3.1.

Table 3.1: Data on Sections 3033 and 3035 of the oil-and-gas flowline

Parameter	Unit	Value of parameter	
		Section 3033	Section 3035
Outer diameter	mm	159	159
Wall thickness	mm	6	6
Length	m	900	2250
Operational pressure	MPa	2.3	2.3
Limiting pressure	MPa	8	8
T, °C	°C	20	20
Total volumetric flowrate	m^3/d	3650	3824
Laying depth	m	1.5	1.5
Outer isolation	-	bitumen enamel	bitumen enamel
Pipeline material	-	Steel St 20	Steel St 20
Inhibitor (currently injected)	-	RIK-1	RIK-1
Injection rate of inhibitor	kg/d	30	30

The accidents are described below in detail:

- Section 3033 rupture (01.01.2021):
    a. reason – pipe flaw 4 mm in diameter caused by internal corrosion;
    b. consequences – oil leakage from underground pipeline 100 m away from valve-30;
    c. amount of spilled liquid – 0.1 m^3;
    d. area of pollution – 1 m^2;
- Section 3033 rupture (13.01.2021):
    a. reason – pipe flaw 3 mm in diameter caused by internal corrosion;
    b. consequences – oil leakage from underground pipeline 200 m away from border of well cluster-2;
    c. amount of spilled liquid – 2 m^3;
    d. area of pollution – 4 m^2;
- Section 3033 rupture (23.03.2021):
    a. reason – pipe flaw 5 mm in diameter caused by internal corrosion;
    b. consequences – oil leakage from underground pipeline 1 m away from valve-34;
    c. amount of spilled liquid – 0.05 m^3;
    d. area of pollution – 1 m^2;

- Section 3035 rupture (19.07.2021):
    a. reason – pipe flaw 3 mm in diameter caused by internal corrosion;
    b. consequences – oil leakage from underground pipeline 300 m away from pig-trap station-8;
    c. amount of spilled liquid – 0.2 m^3;
    d. area of pollution – 5 m^2.

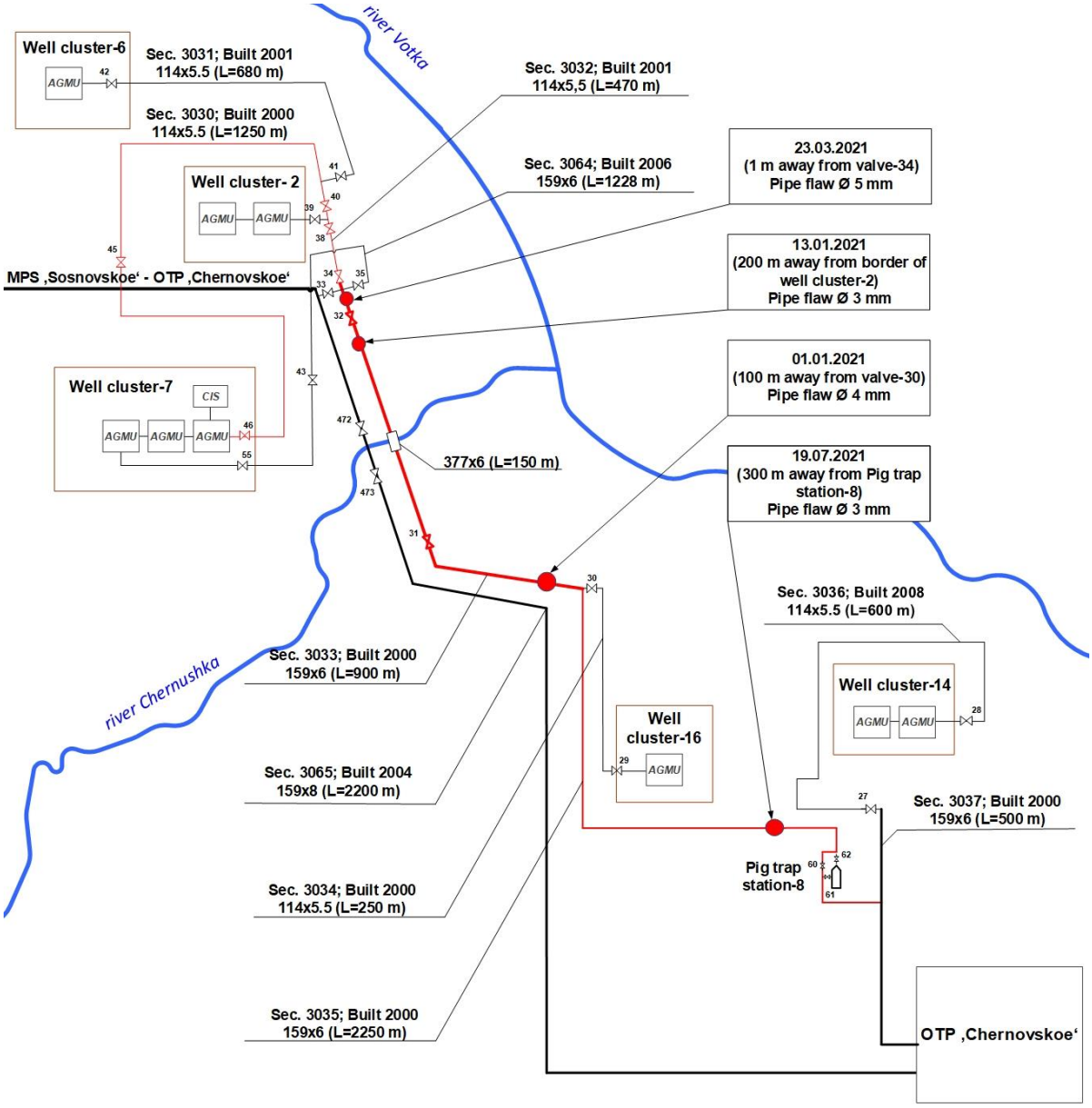

Figure 3.1: Simplified part of scheme of oil-and-gas flowlines of Chernovskoe oilfield

In accordance with the data above, the Section 3033 can be considered as the most problematic segment of oil-and-gas flowline from well cluster-7 to OTP 'Chernovskoe'. It is very important to note that the Section 3033 also has the underwater passage over the river Chernushka. In case of accident, oil spills may pollute the river and cause an ecological disaster.

3.1.1 Input data

It is a well-known fact that more than 80% of oil wells in Udmurt Republic is polluted with H_2S, which affects production processes. Also, high CO_2 content is another negative factor.

In order to analyze the corrosion problem, laboratory tests were conducted by the operating company 'Belkamneft' named after A.A. Volkov, JSC. Hence, fluids that are being transported in the oil-and-gas flowline from well cluster-7 to OTP 'Chernovskoe' were examined. Corrosive tendency is represented in Tables 3.2-3.5. Also, data on a chemical analysis of water is shown in Tables 3.6-3.7.

Table 3.2: Corrosive tendency on 28.01.2021 (sample from Section 3035)

Parameter	Unit	Value of parameter
Corrosion rate	mm/year	0.4043
CO_2 per volume	ppm	7.3
H_2S per volume	ppm	29.2
pH		5.84
HCl per volume	ppm	400

Table 3.3: Corrosive tendency on 14.02.2021 (sample from Section 3030)

Parameter	Unit	Value of parameter
Corrosion rate	mm/year	0.1723
Water cut	wt. %	92
CO_2 per volume	ppm	67.1
H_2S per volume	ppm	5.9
pH		5.97
HCl per volume	ppm	100

Table 3.4: Corrosive tendency on 21.04.2021 (sample from Section 3033)

Parameter	Unit	Value of parameter
Corrosion rate	mm/year	0.1019
Water cut	wt. %	97.6
CO_2 per volume	ppm	135
H_2S per volume	ppm	5.2
pH		5.8
HCl per volume	ppm	100
Soilds per volume	ppm	60
Fe^{3+} per volume	ppm	0.12

Table 3.5: Corrosive tendency on 30.07.2021 (sample from Section 3033)

Parameter	Unit	Value of parameter
Corrosion rate	mm/year	0.0905
Water cut	wt. %	98.1
CO_2 per volume	ppm	45.6
H_2S per volume	ppm	16.2
pH		5.73
HCl per volume	ppm	100
Soilds per volume	ppm	10
Fe^{3+} per volume	ppm	0.34

Table 3.6: Chemical analysis of water on 21.04.2021 (sample from Section 3033)

Parameter	Unit	Value of parameter
Water density	kg/m^3	1180
HCO_3^- per volume	ppm	64.1
Cl^- per volume	ppm	171110
SO_4^{2-} per volume	ppm	511.1
Ca^{2+} per volume	ppm	17635.2
Mg^{2+} per volume	ppm	6000
Na^+ and K^+ per volume	ppm	82840.8
Total salinity	ppm	278161.2
Water hardness	ppm	23635.2

Table 3.7: Chemical analysis of water on 30.07.2021 (sample from Section 3033)

Parameter	Unit	Value of parameter
Water density	kg/m^3	1178
HCO_3^- per volume	ppm	86.6
Cl^- per volume	ppm	169690
SO_4^{2-} per volume	ppm	225.8
Ca^{2+} per volume	ppm	19238.4
Mg^{2+} per volume	ppm	4800
$Mg^{2+}$and K^+ per volume	ppm	82227
Total salinity	ppm	276267.8
Water hardness	ppm	24038.4

According to the data above, corrosion rate varies 0.905-0.4043 mm/year. Determination of corrosion rate was carried out by gravimetric method. The fluid is characterized as the unstable oil-in-water emulsion with solid particles and corrosion products in it. Content of aggressive components in the fluid is pH < 7; CO_2 > 5.0 ppm; H_2S > 1.0 ppm. Thus, in accordance with RD 39-0147103-362-86 (VNIISPTneft, 1987), the fluid is classified as highly-aggressive.

Table 3.8: Field tests of corrosion inhibitors (sample from Section 3035)

Corrosion inhibitor	Mass of a corrosion inhibitor per 1 liter of a fluid, g/L	Corrosion rate, mm/year	Index of corrosion protection
No inhibitor	0	0.4043	0 %
FreeAnCor	0.03	0.1932	52.2 %
SONKOR-9601	0.03	0.2094	48.2 %
RIK-1	0.03	0.1670	58.7 %

In order to prevent subsequent accidents and reduce the corrosion rate, 'Belkamneft' named after A.A. Volkov, JSC requested field tests to be done. A sample of the unstable oil-in-water emulsion from Section 3035 was used for testing of corrosion inhibitors. According to field tests, the corrosion inhibitor RIK-1 performed the best index of corrosion protection of 58.7 % (Table 3.8).

3.2 OLGA

In order to study the hydrodynamic properties of unstable flow in the oil-and-gas flowline, it was decided to use the OLGA simulator by Schlumberger.

OLGA is a dynamic multiphase flow simulator, which models transient flow behavior, providing valuable insights through the entire production system – from reservoir pore to process facility and helps to maximize production potential (Schlumberger Software, 2021).

OLGA consists of two major components – the OLGA GUI and the OLGA simulator. The OLGA GUI is the graphical user interface, which enables the creation of new OLGA cases, editing input, starting simulations, viewing results and much more. The OLGA simulator is the component that performs the simulation. The simulation usually starts from the OLGA GUI, but it can also be started independently by means of a command line interface. The simulation results can be displayed in the OLGA GUI and are stored in plot-files.

An OLGA case is a collection of all the input data that is sent to the simulator when a simulation is run. To simulate the real world objects, it usually consists of pipelines, process equipment and other components. It also contains information about simulation options, initial and

boundary conditions, pressure, temperature and so on, that influence the simulation. A case can also consist of references to other files, such as tab-files (.tab) for fluid definitions and files with compressor characteristics.

An OLGA project is a container for one or more OLGA cases and is a way of organizing relevant files. A project can contain other information, such as Microsoft Office Word documents and reports, Microsoft Office Excel calculations and more. The fluid files that are referred to cases are included in the project automatically.

When working in the OLGA GUI, work is always performed within the context of a project. OLGA creates a project when one does not exist. When a case is opened, the OLGA GUI creates a project for it. When the OLGA GUI is closed, it prompts to save the project and cases.

3.3 Multiflash package for OLGA

The OLGA dynamic multiphase flow simulator also includes a variety of different very helpful external tool packages. One of them is Multiflash. Multiflash is a powerful and versatile system for modelling physical properties and phase equilibria and can be used as a stand-alone program or in conjunction with other software (Infochem/KBC Advanced Technologies Ltd., 2015).

Multiflash can provide:

- all the thermodynamic and transport properties for engineering studies;
- comprehensive fluid characterisation and model tuning for petroleum fluids;
- flash calculations to determine the phases present at specified conditions and their type, composition and amounts;
- complete phase envelopes, showing phase boundaries and critical points;
- modelling solids formation, including pure solids, halide scales, hydrates, waxes and asphaltenes;

Multiflash contains a powerful set of configurable options, which makes it easy to specify all relevant aspects of a study. Each configuration can be saved for future use with Multiflash or other compatible applications (Infochem/KBC Advanced Technologies Ltd., 2015).

3.3.1 Equation of state models

An equation of state (EoS) describes the PVT behaviour of pure components and mixtures. Each EoS represents the attractive and repulsive forces between molecules in different ways. Using an EoS, it is possible to calculate any thermodynamic property relative to the ideal gas properties of the same mixture under the same conditions.

Binary interaction parameters (BIPs) are derived from the regression of experimental phase equilibrium data and allow an EoS to describe any system more accurately. BIPs are adjustable parameters which are used to alter the predictions from a model until these reproduce as closely as possible the experimental data.

An EoS can be used over a wide range of temperature and pressure, including the subcritical and supercritical regions. EoS is frequently used for ideal or slightly non-ideal systems, such as those related to the oil and gas industry, where modelling of hydrocarbon systems containing low density gases, such as H_2S, CO_2 and N_2, is the norm.

However, for highly non-ideal chemical systems, such as alcohol-water, EoS methods are not generally useful. Considering a system of this type, at low pressure an activity coefficient approach is applicable, but at higher pressure an EoS, such as RKSA (Infochem), with excess Gibbs energy mixing rules is more preferable.

From an EoS, thermal properties of any fluid phase can be defined. However, one property which is often poorly represented by the simpler EoS is the liquid density. Multiflash offers enhanced versions of both the Redlich-Kwong-Soave (RKS) and Peng-Robinson (PR) cubic EoS, where the EoS parameters can be fitted to reproduce both the pure component saturated vapour pressure, using a databank correlation, and the saturated liquid density at 298K or Tr = 0.7 (Peneloux method). These are referred to in Multiflash as the advanced version of the particular EoS (Infochem/KBC Advanced Technologies Ltd., 2015).

Multiflash is provided with a comprehensive set of EoS to use different PVT calculations:

- Ideal gas:
    a. brief description: the model is normally used in conjunction with an activity coefficient method when the latter is used to model the liquid phase;
    b. recommended for: gases at low pressure;
- Peng-Robinson (PR):
    a. brief description: a cubic EoS model. The model was designed to calculate the volume of 100% methane gas as a function of pressure and temperature. The equation expresses fluid properties in terms of the critical properties and acentric factor of each species involved (Peng and Robinson, 1976). There is some evidence that this method provides improved volumes and densities compared to RKS.

       The advanced version (PRA) has a choice of mixing rule and includes the ability to match stored values for liquid density and saturated vapour pressure. PRA EoS adds volume translation and a flexible attractive temperature-dependent term to the original PR EoS for accurate PVT and saturation

property correlation for polar compounds. Results of computations show that PRA provides a more detailed description and better understanding of complex dynamic underground fluid phase behavior that may occur during oil recovery processes;

b. recommended for: the original PR is commonly used for gases with high content of methane fraction. PR is insufficiently accurate if there is a water presence in fluid composition. The advanced version (PRA) is suitable for most applications in oil and gas industry;

- Peng-Robinson 1978 (PR78):
  a. brief description: a cubic EoS model. PR78 is the revised version of the PR equation and it has a different treatment for the parameter κ. The defect in the original PR equation where heavy components with higher acentric factors become more volatile than components with lower acentric factors is not present in PR78.

     PR78 gives different results to PR for any mixture containing components with acentric factors greater than 0.49. Consequently, PR78 is classified as a different model.

     The advanced version (PR78A) has a choice of mixing rule and includes the ability to match stored values for liquid density and saturated vapour pressure;
  b. recommended for: the prediction of petroleum fluid phase behavior, behavior of synthetic petroleum fluids including gas injection experiments. The advanced version (PR78A) is suitable for most applications in oil and gas industry;
- Redlich-Kwong (RK):
  a. brief description: a cubic EoS model. The *a* and *b* parameters are expressed explicitly in terms of the critical temperature and pressure;
  b. recommended for: the model is commonly applied in conjunction with an activity coefficient method, which is used to model the liquid phase;
- Redlich-Kwong-Soave (RKS):
  a. brief description: a cubic EoS model. There is some evidence that this method provides improved fugacities compared to PR, PRA, PR78 and PR78A.

     The advanced version (RKSA) has a choice of mixing rule and includes the ability to match stored values for liquid density and saturated vapour pressure;
  b. recommended for: most systems that contain non-polar components, such as petroleum systems and mixtures containing hydrogen;

- Cubic-Plus-Association (CPA):
    a. brief description: a cubic EoS model. Three variants are currently available in Multiflash: CPA-Infochem, CPA-PRA78 and CPA-DTU. Each variant contains a cubic term that is RKSA, PR78A or RKS respectively, plus an additional term based on Wertheim's theory, that represents the effect of chemical association. For non-polar components, all CPA variants reduce to their cubic EoS.

       The Peneloux density correction is used in CPA-Infochem and CPA-PRA78 in order to match the liquid density and volume calculated from the EoS to that stored in the chosen physical property data system;
    b. recommended for: cases of industrial importance, such as hydrate calculations and other fluids containing water, hydrocarbons, methanol, ethanol, MEG, DEG, TEG, organic acids and salts. Also, CPA is suitable for the estimation of pure compound parameters, alcohol-hydrocarbon vapour-liquid equilibria (VLE), solid-liquid equilibria (SLE) and aqueous systems;
- Predictive Soave-Redlich-Kwong (PSRK):
    a. brief description: a cubic EoS model. The model includes the RKSA EoS with vapour pressure fitting, the Peneloux density correction and the PSRK type mixing rules.

       PSRK enables the estimation of properties of mixtures containing supercritical components. PSRK is similar to the normal VLE UNIFAC model, which is a semi-empirical system for the prediction of non-electrolyte activity in non-ideal mixtures, except that the group table has been extended to include a large number of common low density gases;
    b. recommended for: estimation of phase equilibria of mixtures of chemical components, such as fluids with polar liquids and estimation of properties of mixtures containing supercritical components;
- Zudkevitch-Joffe (ZJ):
    a. brief description: a cubic EoS model. A variant of the original RK EoS. The a and b parameters are defined by solving the equation of pressure for both gaseous and liquid phase and equations of fugacity coefficients along the saturation line simultaneously. The default BIPs in Multiflash are not regressed against any experimental data. Hence, suitable BIPs are required in order to use the model effectively;
    b. recommended for: simulation of laboratory PVT experiments, where each PVT experiment represents a phase behavior progression for a reservoir fluid from

a reservoir to surface facilities with improved predictions on enthalpy for both saturated and compressed liquids;

- Perturbed Chain Statistical Associating Fluid Theory (PC-SAFT):
    a. brief description: the model incorporates current ideas of accurate and detailed modeling of fluid thermodynamics. PC-SAFT follows the same general structure as the association term in the CPA model. Also, the dipolar and quadrupolar terms are included when the dipole moment and quadrupole moments are available;
    b. recommended for: polymer systems, most polar and non-polar systems;
- PC-SAFT simplified:
    a. brief description: the model is similar to PC-SAFT but has simplified mixing rules proposed by Danish Technical University. The model uses the same pure component parameters as PC-SAFT, but BIPs of the model are different;
    b. recommended for: polymer systems, most polar and non-polar systems;
- Lee-Kesler (LK) and Lee-Kesler-Plöcker (LKP):
    a. brief description: LK and LKP are 3-parameter corresponding states methods, which are based on interpolating the reduced properties of a mixture between the reduced properties of two reference substances.

    LK and LKP are used for prediction of fugacity coefficients, thermal properties and volumetric properties of a mixture. Nevertheless, LK and LKP are rather slow and complex compared to the cubic EoS and are not recommended for phase equilibrium calculations;
    b. recommended for: precise calculations of density and enthalpy of non-polar and mildly-polar mixtures, such as hydrocarbons and low density gases;
- Benedict-Webb-Rubin-Starling (BWRS):
    a. brief description: an 11-parameter non-cubic EoS. The model provides reasonable VLE predictions only if suitable BIPs are given.

    For methane, ethane, ethylene, propane, propylene, iso-butane, n-butane, iso-pentane, n-pentane, hexane, heptane, octane, carbon dioxide, hydrogen sulphide and carbon dioxide, the pure component parameters are set to values recommended by Starling (Starling, 1973). For other substances, the pure component parameters are defined by means of correlations created by Starling and Han (Starling, 1973).

    However, Multiflash does not provide many BIPs in its databank. Due to complexity of BWRS, it requires more computing time than a cubic EoS;

   b. recommended for: precise calculations of volumetric and thermal properties of low density gases and hydrocarbons;

- Multi-reference fluid corresponding states (CSMA):
   a. brief description: the model is based on a collection of very accurate EoS for a number of reference fluids. CSMA uses a one-fluid corresponding states approach to estimate mixture properties and allows to obtain precise magnitudes of thermodynamic properties for any of reference fluids. Hence, as composition of a mixture approaches limits for each pure component, properties of a mixture are reduced to values of pure components;
   b. recommended for: any mixture of the reference fluids;
- GERG-2008:
   a. brief description: an industry-standard high-accuracy model for mixtures which consist of natural gas components. The model includes appropriate BIPs for all components in the Geochemical and Environmental Research Group (GERG) reference list.

      GERG-2008 performs best for mixtures without strong specific interactions and for any of pure reference substances. The mixture model is applicable to systems that do not contain free water.

      GERG-2008 is a well-verified standard. It is classified as the best model for natural gas mixtures containing the GERG reference components (Kunz, Klimeck, Wagner, Jaeschke, 2007);
   b. recommended for: natural gas pipelines and processes, CO_2 transportation, carbon sequestration, acid gas injection, water or steam systems, air, instrument calibration and multi-phase meters;
- GERG-2008 (Infochem extension):
   a. brief description: the extended version of GERG-2008 is a pseudo reference EoS for petroleum fractions or components for which high-accuracy EoS are not available.

      For a component or a peseudocomponent in a mixture with no high-accuracy EoS, a four-parameter corresponding-states principle (CSP) model proposed by Sun and Ely in 2005 is used to generalize the universal technical EoS. The CSP model in Multiflash is implemented by means of Helmholtz free energy. Moreover, reference fluids for non-polar or weakly-polar components are two non-spherical fluids of propane and octane (Sun, Ely, 2005).

   b. recommended for: modelling a fluid phase behaviour of low density condensates with small amount of impurities and mixtures with components, for which high-accuracy EoS are not available;
- Water high accuracy:
   a. brief description: the model comprises the reference IAPWS95 EoS of Wagner & Pruß and high-accuracy models for the transport properties of water;
   b. recommended for: any fluid where water properties are critical to calculation;
- Carbon dioxide high accuracy:
   a. brief description: the model comprises the reference EoS of Span & Wagner and high-accuracy models for the transport properties of carbon dioxide;
   b. recommended for: any fluid where the carbon dioxide properties are critical to calculation;
- COSTALD:
   a. brief description: a corresponding states method for estimating the density of liquid mixtures. The method predicts high-accuracy volumes for pure substances and simple mixtures, such as LNG. However, the method is not recommended for heavy hydrocarbon mixtures with dissolved gases;
   b. recommended for: compressed liquids and liquids on the saturation line.

3.3.2 Defining fluids in Multiflash

In Multiflash, a fluid is the mixture of components on which calculations are carried out. The definition of a fluid is extremely significant to use Multiflash successfully.

Any fluid can be defined in different ways:

- mixture of standard components – a standard fluid comprises standard components available in Multiflash. Up to 200 components can be specified in a standard fluid;
- set of petroleum fractions – a complex mixture of hydrocarbons with aggregate properties defined by standard tests. Results of these tests may be taken from PVT laboratory reports or from other process simulation software. Up to 100 petroleum fractions can be specified;
- mixture of standard components and petroleum fractions;
- petroleum fluid characterized by a PVT laboratory analysis – a comprehensive compositional analysis of a fluid, usually carried out by gas chromatography;
- petroleum fluid characterized from experimental distillation data – applied when input PVT analysis data is based on true boiling point (TBP) curve or a D86 analysis. The data may be entered and converted to single carbon number fractions (SCN):

a. true boiling point (TBP) distillation data:
    1. cumulative percentage distilled by volume;
    2. fraction boiling point;
    3. measured molecular weight of fraction (optional);
    4. measured specific gravity of fraction (optional);
b. D86 analysis – is a standard analytical procedure. An oil sample is placed in a single vessel and progressively heated to separate a gas from it. Multiflash converts D86 data into equivalent TBP data using the method of Riazi and Daubert (Riazi, Daubert, 1986). D86 distilation data includes:
    1. cumulative percentage distilled by volume;
    2. fraction boiling point;

- petroleum fluid characterized from limited data (black oil analysis) – it enables to define a fluid when a compositional data is very limited. The analysis is very useful in cases if a PVT analysis is not available or the data is generated from another application.
- blend of previously characterized petroleum fluids – user-defined components may be added if the required component is absent in the Multiflash database.

3.3.2.1 Defining fluids using a PVT laboratory analysis

PVT laboratory analysis – is a compositional analysis of a fluid, usually carried out by gas chromatography. Gaseous and liquid phases from a separator test or bottom-hole sample are analyzed separately. The results are usually recombined in order to define composition of a reservoir fluid.

PVT laboratory analysis usually includes the following:

- light hydrocarbons and inorganic compounds, such as N_2, CO_2 and H_2S, are identified individually;
- single carbon number fractions (SCN) - the analysis for hydrocarbons with more than six or seven carbon atoms, which represents compounds in boiling point ranges. For instance, a C8 SCN contains all hydrocarbons that boil between the normal boiling point of n-heptane +0.5 ºC, and the normal boiling point of n-octane +0.5 ºC;
- the analysis stops at a carbon number that is reported as a plus fraction. A plus fraction is the highest number SCN fraction in a fluid, which contains all the material in the heavy end of the fluid and often represents a substantial proportion of the fluid. For instance, C25+;
- as an option, the n-paraffin content analysis may be conducted.

Characterization – is the use of the data from a PVT laboratory analysis report to create a compositional fluid model in Multiflash. Characterizing a petroleum fluid is an essential pre-requisite to study the phase behaviour and other properties of the fluid.

Objectives of the Multiflash characterization procedure are:

- make optimum use of measured data.
- create a compositional model that is not restricted to a particular thermodynamic model under consideration.
- ensure that phase behaviour calculations are not sensitive to the number of pseudocomponents, which are a kind of set of petroleum SCN fractions that are aggregated together;
- achieve high fidelity based on compositional information;
- allow model tuning to reproduce reliable experimental measurements.

There are different characterization options available in Multiflash. Each of them has different purposes:

- Single Fluid – a recombined reservoir fluid analysis;
- Gas and Liquid – a separator gas and separator liquid analysis;
- Single Fluid and N-Paraffins (STO) – a recombined reservoir fluid analysis plus an analysis of the n-paraffin distribution measured for the STO;
- Single Fluid and N-Paraffins (fractions) – a recombined reservoir fluid analysis plus an analysis of the n-paraffin distribution described as the fraction of each individual n-paraffin, which is SCN above C6;
- Gas, Liquid and N-Paraffins (STO) – a separator gas and separator liquid analysis plus an analysis of the n-paraffin distribution in the liquid phase measured for the STO;
- Gas, Liquid and N-Paraffins (fractions) – a separator gas and separator liquid analysis plus an analysis of the n-paraffin distribution in the liquid phase described as the fraction of each individual SCN above C6 which is n-paraffin.

3.3.2.2 Phase diagram

Multiflash is capable of handling up to twenty phases at any time, but the maximum which can exist together at equilibrium is limited to seven.

The phase types that are included in Multiflash are:

- vapour;
- liquid;
- pure solid;
- fixed composition solid;

- hydrate;
- wax;
- asphaltene;

More than one of all these types can co-exist, except for vapour. Nevertheless, more than one wax or asphaltene phase may be defined due to the structure of software and models. Each phase is identified by means of names and key components.

There are significant parameters, which are determined using a phase diagram (Figure 3.2):

- critical point – the point where gaseous and liquid phases have identical density and composition. However, the liquid-liquid critical point, where two liquid phases are indistinguishable, also exists;
- cricondentherm – the maximum temperature at which a two-phase mixture can exist;
- cricondenbar – the maximum pressure at which a two phase mixture can exist;
- bubble point – the pressure at which light components no longer remain dissolved in heavier liquid components and start to separate as a gas;
- retrograde dew point – the point at which liquids drop out of the gaseous phase. If the amount of liquid increases as the pressure decreases, then the phenomenon of retrograde condensation occurs.

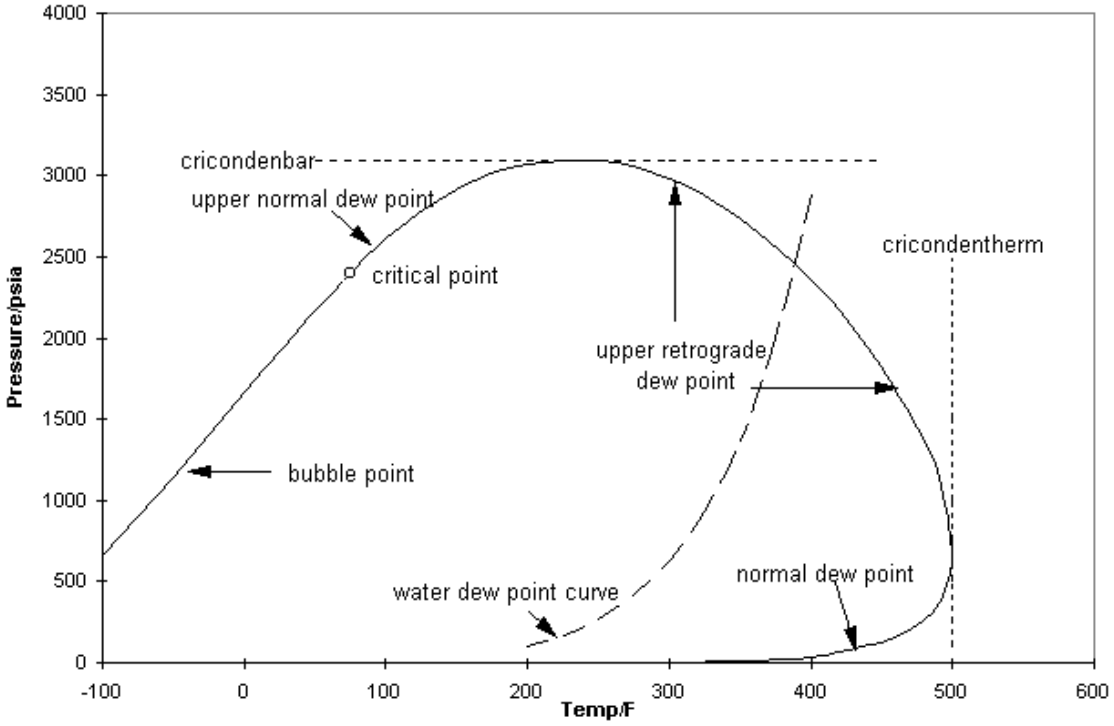

Figure 3.2: Phase diagram for a gas condensate

3.3.3 Blending fluids in Multiflash

Creating a blended fluid is useful when two or more fluids mix in cases, such as pipes intersection. Existing, characterized fluids can be blended in order to create a new fluid that is characterized by its own set of components and pseudo-components. The properties and relative amounts of the blended pseudo-components of fluid are calculated automatically by Multiflash.

The blending method is a way to combine previously defined fluids within Multiflash. It works for any type of fluid that can be represented in Multiflash and saved in a .mfl file. It works best if the fluids and the pseudo-component distributions are similar.

The blending method works as follows:

- identify the pure components from each fluid used, and add them together in specified proportions;
- identify the dominant pseudo-components from each fluid used, and add them to the new mixture;
- the dominant pseudo-components – are components, which have the highest concentration in a mixture for each range of molecular weight and are the main part of molecular weight distribution;
- the remaining pseudo-components are then added to the most physically similar dominant pseudo-components and average physical properties of the resulting blended pseudo-components are obtained.

The blending method has the following advantages:

- automatic and no user intervention is required;
- properties of a blended fluid change smoothly with changing blend ratios as well as properties of unblended fluids, but only if small amounts of other fluids are added;
- the method of averaging properties of blended pseudo-components is exactly the same as the pseudo-components creation used in a PVT laboratory analysis;
- the method works well with waxy and asphaltenic crudes and also predicts the likelyhood of wax or asphaltene formation from a blended fluid.

The blending tool and the same pseudos tool perform a similar function. However, there are significant differences between blending and characterizing multiple fluids:

- the blending tool produces the Single Fluid, while the same pseudos tool produces a fluid for each input fluid;
- lumped components without considering the original characterization are used by blending tool. Hence, a plus fraction for each fluid is maintained;

- blending tool does not make use of PVT experimental data, therefore model tuning can not be performed after blending.

3.4 PIPESIM

To study corrosion processes of unstable flow in the oil-and-gas flowline, the PIPESIM simulator by Schlumberger was used.

The PIPESIM simulator provides the most advanced steady-state modeling capabilities in the industry to fulfill critical aspects of a study.

A wide variety of industry-standard multiphase flow correlations, as well as advanced 3-phase mechanistic models, including OLGA-S, Kongsberg LedaFlow Point Model, and the TUFFP unified model are incorporated by the PIPESIM simulator. Hence, it provides possibility of calculation of flow regimes, liquid holdup, slug characteristics, and pressure loss for all nodes along production paths of all deviations. This data is extremely important for designing and operating production gathering and distribution systems. Moreover, a detailed flow regime maps at points of interest is produced by the PIPESIM simulator.

An accurate description of fluid behavior is critical to model the production system correctly. The PIPESIM simulator has a range of models from the industry-standard black-oil correlations to a range of EoS compositional models. In addition, the ASTM97 Steam Tables allow the steam to be modeled as a single component system.

PVT-files can be generated by some Schlumberger and third-party applications. PVT-files can be used by the PIPESIM simulator to interpolate fluid and transport properties. These applications include:

- Multiflash (Infochem);
- PVTSim (Calsep);
- HYSYS (Aspentech);
- UniSim (Honeywell);
- ScaleChem (OLI Systems);
- dbrSOLIDS fluid analysis software (Schlumberger);
- GUTS (MSI);
- AsphWax.

3.4.1 de Waard corrosion model

The de Waard corrosion model predicts the corrosion rate of carbon steel in the presence of water and CO_2. (de Waard, Lotz and Dugstad, 1995). The model was invented primarily for use in predicting corrosion rates in pipelines where CO_2 is present in a gaseous phase and was not validated at high pressures where CO_2 is entirely in a liquid phase.

Corrosion rate in the de Waard corrosion model is calculated as a function of:

- temperature;
- pressure;
- CO_2 (mol. %);
- glycol (wt. %) – Multiflash and ScaleChem only;
- liquid velocity;
- pipe diameter;
- pH.

The de Waard corrosion model accounts for both flow-independent kinetics of the corrosion reaction and flow-dependent mass transfer of dissolved CO_2 by means of a resistance model. Also, effects of protective scale at high temperatures are considered as well as glycol reduction effect.

General equation for de Waard corrosion model:

$$V_{cor} = \frac{Cc \cdot \mathrm{Fs} \cdot \mathrm{Fg}}{\frac{1}{V_r} + \frac{1}{V_m}} \tag{3.1}$$

where V_{cor} is the corrosion rate (mm/year); Cc is the multiplier to correct for inhibitor efficiency or match to field data; Fs is the scaling factor; Fg is the glycol reduction effect; V_r is the reaction rate term (mm/year); V_m is the mass transfer rate term (mm/year).

CO_2 partial pressure is calculated as shown in equation (3.2):

$$pCO_2 = \frac{nCO_2 \cdot P_{total}}{100} \tag{3.2}$$

where pCO_2 is the partial pressure of CO_2 (atm); nCO_2 is the mole fraction of CO_2; P_{total} is the total pressure (atm).

CO_2 fugacity is calculated as shown in equation (3.3):

$$\log(fCO_2) = \log(pCO_2) + \left(0.0031 - \frac{1.4}{T}\right) \cdot P_{total} \tag{3.3}$$

where fCO_2 is the fugacity of CO_2 (atm); T is temperature (K).

Reaction rate term is calculated as shown in equation (3.4):

$$\log(V_r) = 4.93 - \frac{1119}{T} + 0.58 \cdot \log(fCO_2) - 0.34\left(pH_{act} - pH_{CO_2}\right) \tag{3.4}$$

where pH_{act} is the actual pH of the system; pH_{CO2} is the pH of dissolved CO_2 in pure water.

By default, the correlation assumes that the actual pH of water is affected strictly by the presence of CO_2. But the actual pH of water can be specified too. In general, pH accounts for the additional presence of electrolytes and dissolved $FeCO_3$ liberated from the pipe wall. Magnitudes of pH also depend on pressure and temperature.

pH of dissolved CO_2 in pure water is calculated as shown in equation (3.5):

$$pH_{CO_2} = 3.82 + 0.00384 \cdot (T - 273) - 0.5 \cdot \log(fCO_2) \tag{3.5}$$

Mass transfer rate term is calculated as shown in equation (3.6):

$$V_m = 2.45 \cdot \frac{U_L^{0.8}}{d^{0.2}} \cdot fCO_2 \tag{3.6}$$

where U_L is the liquid velocity (m/s); d is the pipe diameter (m).

Scaling factor, which is dependent on corrosion rate inversion temperature is calculated as shown in equations (3.8-3.9):

$$Ts = \frac{2400}{6.7 + 0.44 \cdot \log(fCO_2)} \tag{3.7}$$

$$\begin{cases} \log(Fs) = 2400 - \left(\frac{1}{T} - \frac{1}{Ts}\right) & if\ T > Ts \quad (3.8) \\ Fs = 1 & if\ T < Ts \quad (3.9) \end{cases}$$

where Ts is the corrosion rate inversion temperature (K).

The glycol component is only available when using Multiflash (MEG or DEG) or with ScaleChem (MEG). Glycol reduction effect is calculated as shown in equation (3.10):

$$\log(Fg) = 1.6 \cdot (\log(WC) - 2) \tag{3.10}$$

where WC is the water cut (wt. %).

Chapter 4

Calculations of unstable flow in oil-and-gas flowline

4.1 Calculations in Multiflash

In order to analyze the unstable oil-in-water emulsion, Multiflash was used to create a fluid. The data from Production Department of 'Belkamneft' named after A.A. Volkov, JSC was requested to find a solution of the problem.

At first, the field development maps of Chernovskoe oilfield were used to define wells which are connected to the oil-and-gas flowline from well cluster-7 to OTP 'Chernovskoe' which is under consideration in the Thesis. According to the data from Production Department, there are 41 wells connected to the oil-and-gas flowline from well cluster-7 to OTP 'Chernovskoe'. The wells are located on four different well clusters: well cluster-2 (13 wells), well cluster-6 (2 wells), well cluster-7 (24 wells), well cluster-16 (2 wells). Five wells are dual completion wells. Three oil-bearing horizons are operated by the wells – Vereiskian-Bashkirian (V-B), Visean (V) and Tournai (T), as shown in Table 4.1.

According to the data from Table 4.1, total flowrates of oil (Q_{oil}) and water (Q_{water}) can be defined per each oil-bearing horizon (Table 4.2). But it is very important to mention that the data on flowrates was vaild on 01.01.2016. Consequently, current flowrates differ, but flowrates are represented here to have an idea of distribution of oil and water from different oil-bearing horizons.

Table 4.1: Data from Production Department on wells connected to the flowline from well cluster-7 to OTP 'Chernovskoe'

Well cluster number	Well number	Oil-bearing horizon	Q_{oil}, m^3/d	Q_{water}, m^3/d	Water cut, wt. %
7	3B	V-B	3.5	4	53.333
7	101	V-B	10.3	49.4	82.747
7	103	V-B	11.9	6.3	34.615
7	106	V-B	4.6	120.6	96.326
2	107	V-B	0.3	17.5	98.315
2	108	V-B	7.5	13.5	64.286
7	109	V-B	3.2	33.4	91.257
2	110	V-B	4.7	53.3	91.897
7	171	V-B	2.4	6.3	72.414
7	172	V-B	3.4	35.8	91.327
2	173	V-B	4.4	2	31.250
7	176	T	15.6	281	94.740
7	202	V-B	7.3	3.5	32.407
6	203	V-B	3.7	30.3	89.118
7	207	V-B	2.5	13.7	84.568
7	210	V-B	3.9	23.7	85.870
7	211	V-B	1.6	34.3	95.543
2	212	V-B	6.2	4.2	40.385
16	215	V-B	2.2	40.3	94.824
16	216	V-B	1.4	41.4	96.729
7	271	V-B	13.5	8.4	38.356
7	272	V-B	10.2	6.1	37.423
2	273	V-B	2.5	38.4	93.888
2	276	V-B	1.3	7.8	85.714
7	301	V	9.6	3.8	28.358
2	302	V-B	1.2	17.2	93.478
2	303	V-B	2	17.5	89.744
7	304	V	4.8	5.2	52
		T	4.1	125.7	96.841
2	305	V	5.8	28.6	83.140
		T	4.1	122.8	96.769
7	306	T	7.5	171.1	95.801
7	310	V-B	2.4	5.1	68.000
7	314	V	0.6	30.4	98.065
7	315	V	14.6	350.9	96.005
7	401	V-B	6.8	3.2	32
2	402	V	6.7	24.8	78.730
		T	1.8	91.5	98.071
7	403	V	26.2	338.8	92.822
2	404	V	15.2	9.5	38.462
7	405	V-B	3.8	23	85.821
		V	1.7	79.1	97.896
7	407	V	4.1	7.7	65.254
6	408	V-B	4.3	4.9	53.261
		T	14.1	12.2	46.388
2	410	T	2.2	4.9	69.014

Table 4.2: Summarized data on flowrates

Oil-bearing horizon	Q_{oil}, m^3/d	Q_{water}, m^3/d	$Q_{oil+water}$, m^3/d	Average water cut, wt. %
Vereiskian-Bashkirian	129.5	661.1	790.6	83.620
Visean	89.3	878.8	968.1	90.776
Tournai	49.4	809.2	858.6	94.246
Summary	268.2	2349.1	2617.3	89.753

The data above will be used to analyze if volume ratios of oil and water from different oil-bearing horizons changes properties of the unstable oil-in-water emulsion, which is under research. To perform further analysis in Multiflash, the data on oil and gas composition was requested from Production Department (Tables 4.3-4.4). It is very significant to mention that the information below do not include any data on H_2S content in oil and gas.

Table 4.3: Data from Production Department on oil composition

Parameter	Units	Oil-bearing horizon			
		Vereiskian	Bashkirian	Visean	Tournai
Reservoir pressure	MPa	12.3	12.3	14.9	16.1
Bubble point pressure	MPa	4.5	4.5	4.1	5.1
Reservoir temperature	°C	24	24	24	24
Density of live oil	kg/m^3	870	881	903	915
Density of dead oil	kg/m^3	892.2	906.7	905.2	918.2
Viscosity of live oil	mPa·s	10-17	21.6	37.5	98.4
GOR	m^3/t	16.9	15.2	7.2	7
Wax melting temperature	°C	50.4	50.8	52	51.4
Asphaltenes	mol. %	3.72	4.8	4.2	4.65
Resins	mol. %	21.08	20.23	23.5	22.89
Waxes	mol. %	2.74	3	3.8	2.46
Sulfur	mol. %	2.85	3.09	2.72	2.79

Table 4.4: Data from Production Department on gas composition

Parameter	Units	Oil-bearing horizon			
		Vereiskian	Bashkirian	Visean	Tournai
CH_4	mol. %	10.66	6.95	8.54	2.52
C_2H_6	mol. %	14.32	7.21	11	2.87
C_3H_8	mol. %	25.63	15.27	17.44	6.95
i-C_4H_{10}	mol. %	4.31	4.3	4.26	1.62
n-C_4H_{10}	mol. %	9.59	7.34	6.69	2.25
i-C_5H_{12}	mol. %	3.18	2.47	2.22	0.42
n-C_5H_{12}	mol. %	2.41	1.31	1.33	0.25
C_{6+}	mol. %	1.31	0.63	0.5	0.1
CO_2	mol. %	1.68	5.85	0.655	0.1
N_2	mol. %	26.87	48.67	47.33	82.9
He	mol. %	0.04	0	0.035	0.02
Specific gravity of gas		1.3486	1.213	1.282	1.074

Based on the data from Tables 4.3-4.4, eight separate .mfl files were created for oil and gas. A PVT laboratory analysis was used to model four gases. However, fluids were characterized as the Single Fluid, as shown in Figure 4.1.

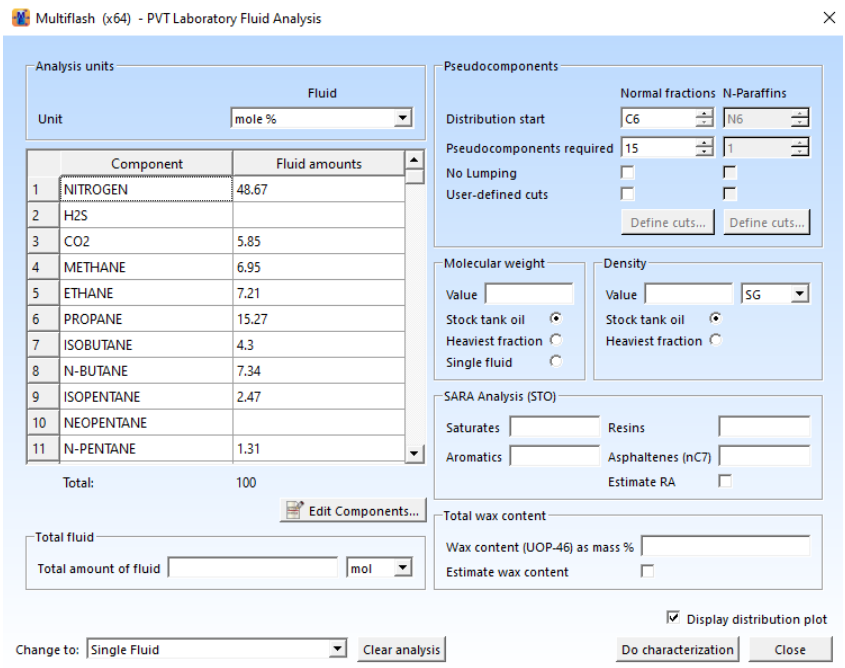

Figure 4.1: PVT laboratory analysis to define gas in Multiflash

Black oil analysis was implemented to create four oil models, as there is no sufficient data on oil composition to be used, but density of dead oil, total wax content and some figures from

SARA analysis (Figure 4.2). EoS model applied to all the fluids was decided to be PRA, as it shows sufficiently accurate results in most petroleum cases.

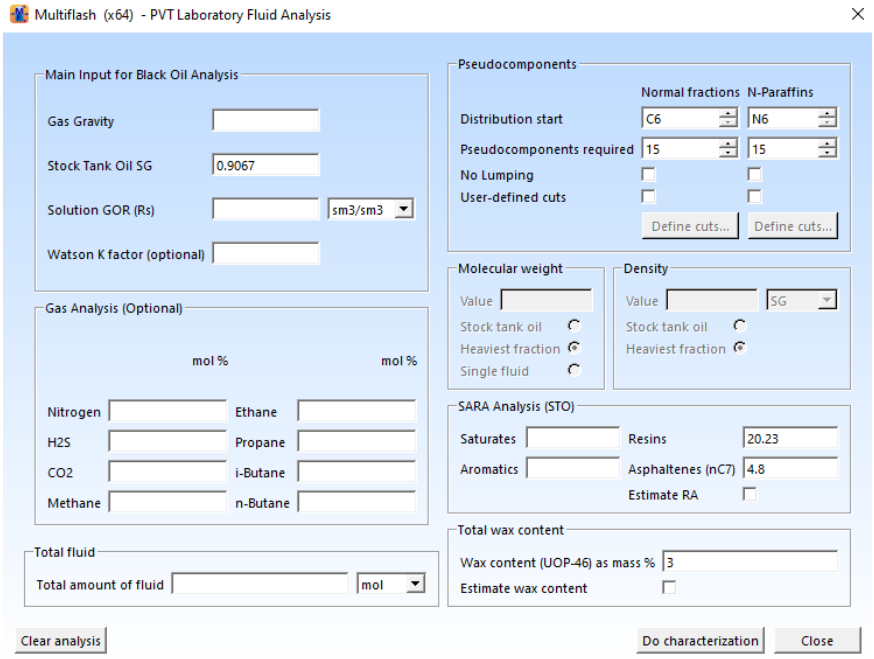

Figure 4.2: Black oil analysis to define oil in Multiflash

Therefore, eight .mfl files defining oil and gas from which the unstable oil-in-water emulsion consists of have been created successfully. After that, it was necessary to blend Vereiskian and Bashkirian oil and Vereiskian and Bashkirian gas in equal proportions to get a Vereiskian-Bashkirian oil and a Vereiskian-Bashkirian gas respectively. For this purpose, Blend Fluids option was used in Multiflash.

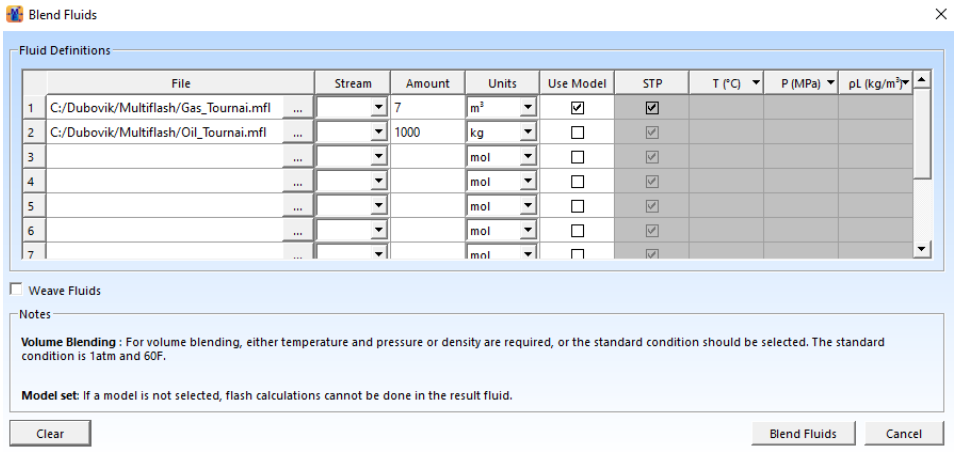

Figure 4.3: Blend Fluids option in Multiflash

Consequently, six necessary .mfl files existed at this step. Then, in accordance with GOR magnitudes, Blend Fluids option was used to create three oil-and-gas mixtures:

Vereiskian-Bashkirian oil-and-gas mixture, Visean oil-and-gas mixture and Tournai oil-and-gas mixture (Figure 4.3).

However, influence of water cut on properties of oil-and-gas mixture had to be considered. Moreover, it is important to define if ratios of oil, water and gas from each oil-bearing horizon influence on properties of the unstable oil-in-water emulsion. To do this, each of three oil-and-gas mixtures were saturated with different amount of water. Water was added as a standard component in Multiflash. It was decided to observe five different water cuts of 30, 45, 60, 75, 90 wt. % for each oil-and-gas mixture. Hence, 15 more .mfl files were created.

As a result, three phase diagrams were plotted to compare properties of each oil-and-gas mixture (Figures 4.4-4.6). The Phase Envelope option in Multiflash was used for this purpose.

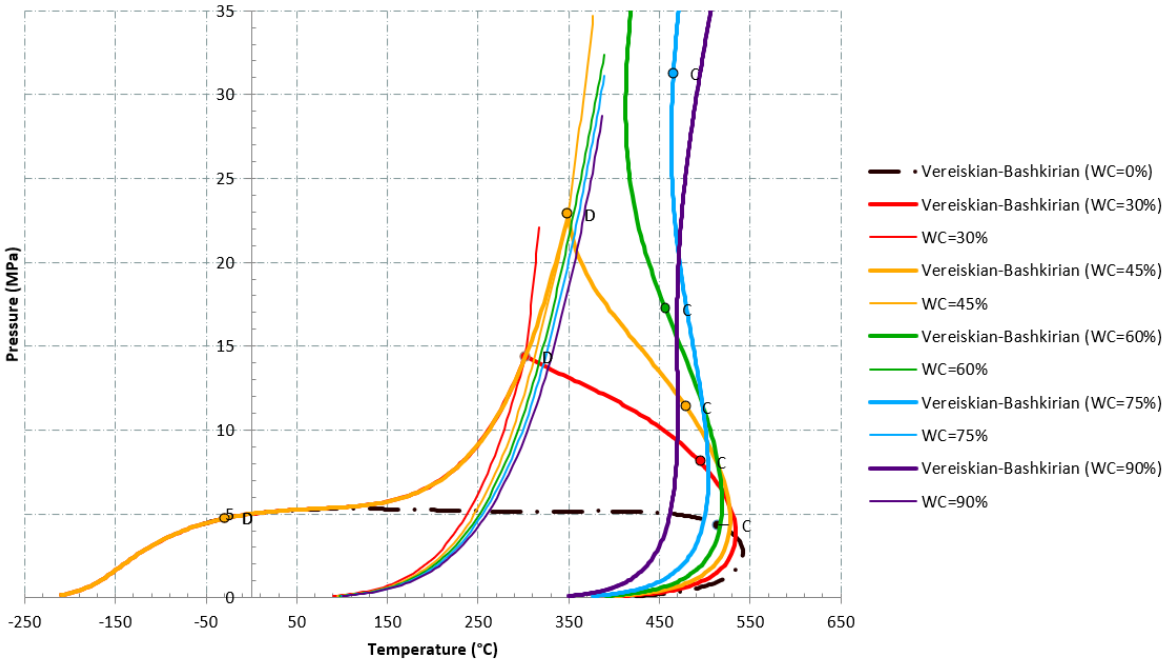

Figure 4.4: Phase diagrams for Vereiskian-Bashkirian oil-and-gas mixtures with different water cuts

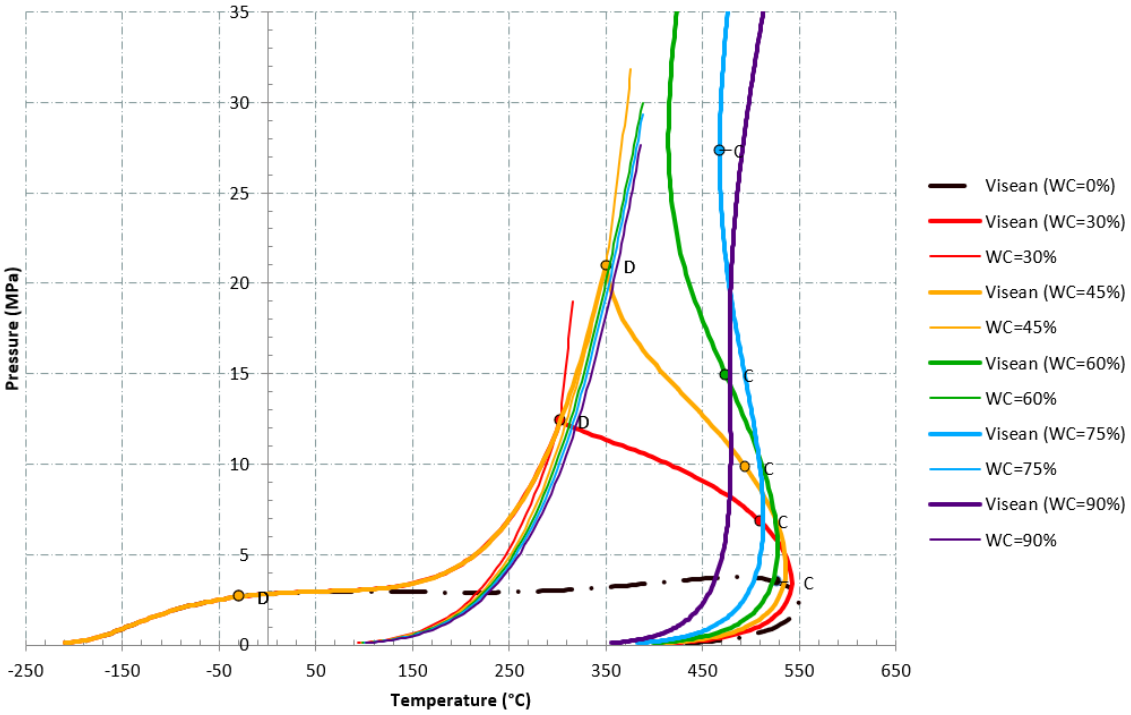

Figure 4.5: Phase diagrams for Visean oil-and-gas mixtures with different water cuts

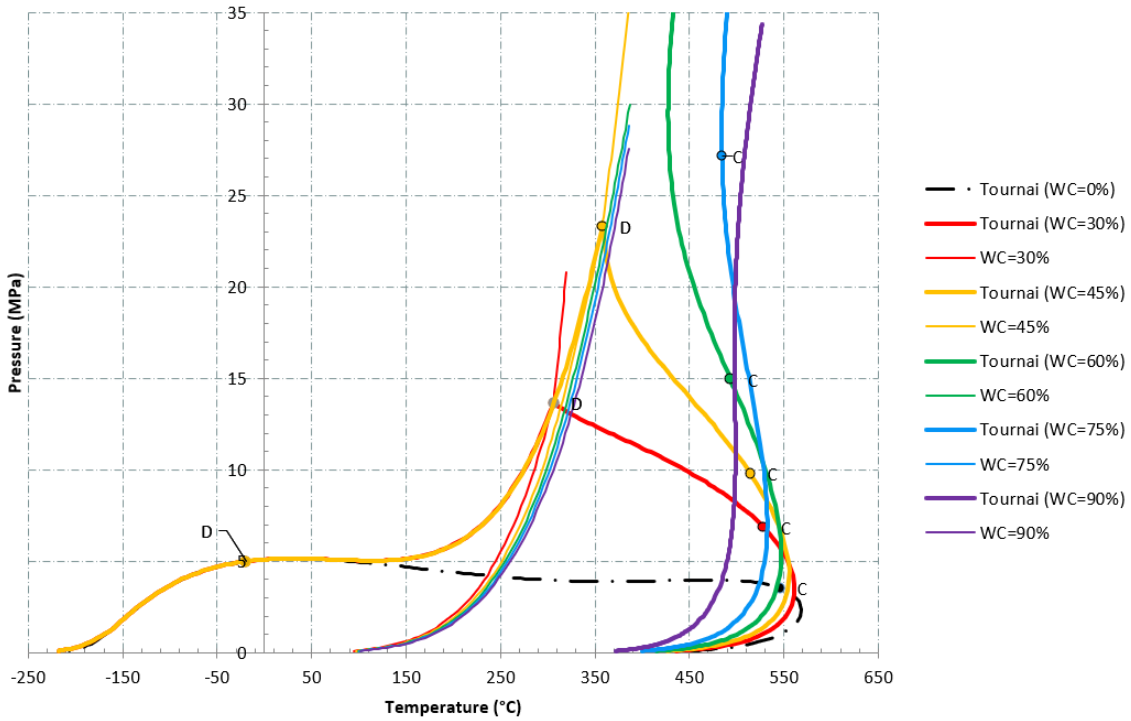

Figure 4.6: Phase diagrams for Tournai oil-and-gas mixtures with different water cuts

As shown in Figures 4.4-4.6, there are almost no differences in behavior of phases of each oil-and-gas mixture.

The next step was to blend oil-and-gas mixtures with water cut of 90 wt. % using every possible flowrate combination of 0.7·Q (min), Q (average) and 1.3·Q (max), as shown in Table 4.5. The objective is to define if fluid properties change in case of presence of different proportions of each oil-and-gas mixture.

Table 4.5: All sorts of flowrate combinations for oil-and-gas mixtures

Name of fluid	Oil-bearing horizon		
	V-B	V	T
111	Max	Max	Max
112	Max	Max	Average
113	Max	Max	Min
121	Max	Average	Max
122	Max	Average	Average
123	Max	Average	Min
131	Max	Min	Max
132	Max	Min	Average
133	Max	Min	Min
211	Average	Max	Max
212	Average	Max	Average
213	Average	Max	Min
221	Average	Average	Max
222	Average	Average	Average
223	Average	Average	Min
231	Average	Min	Max
232	Average	Min	Average
233	Average	Min	Min
311	Min	Max	Max
312	Min	Max	Average
313	Min	Max	Min
321	Min	Average	Max
322	Min	Average	Average
323	Min	Average	Min
331	Min	Min	Max
332	Min	Min	Average
333	Min	Min	Min

In accordance with Table 4.5, fluids 111, 222 and 333 have similar composition, but different volume. Thus, they were observed as a single case. As a result, 27 more .mfl files were created.

As a result, 27 more .mfl files were created. Also, 27 phase diagrams were plotted to compare properties of each oil-and-gas mixture (Figure 4.7). The Phase Envelope option in Multiflash was used for this purpose.

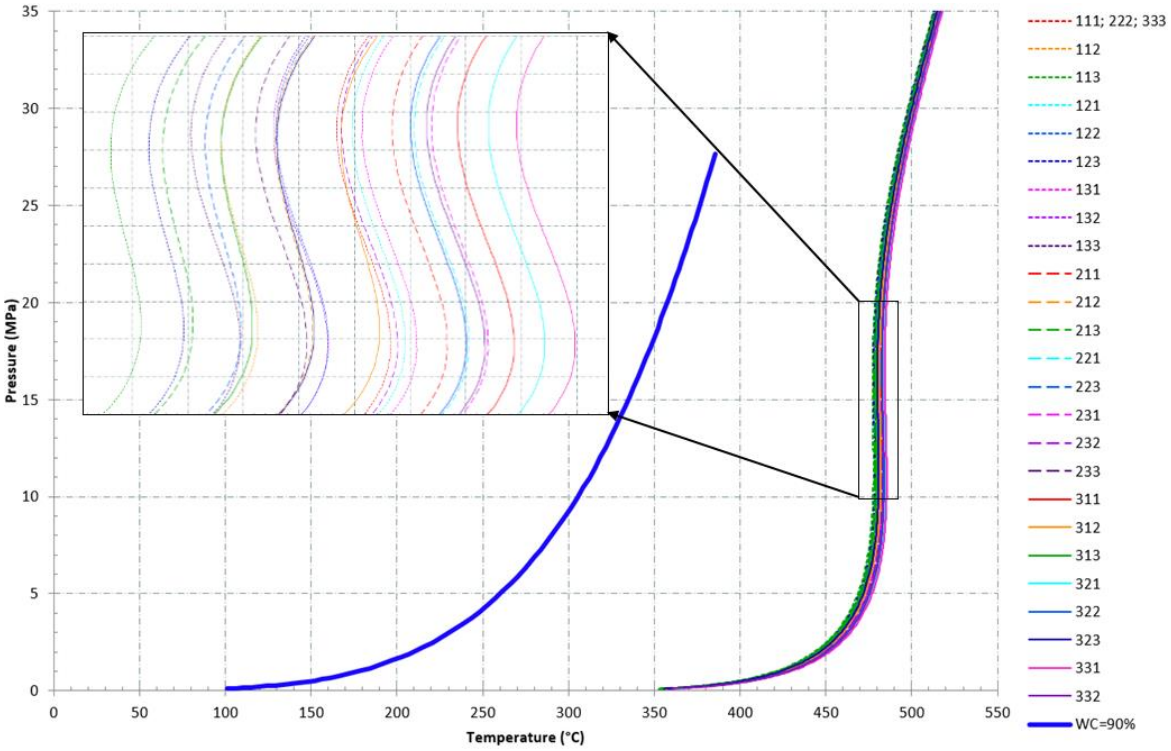

Figure 4.7: Phase diagrams for different proportions of oil-and-gas mixtures from Vereiskian-Bashkirian, Visean and Tournai oil-bearing horizons with water cut of 90 wt. %

As shown in Figure 4.7, if oil-and-gas mixtures from Vereiskian-Bashkirian (V-B), Visean (V) and Tournai (T) oil-bearing horizons with water cut of 90 wt. % are mixed in different proportions, fluid properties do not differ significantly. Thus, the mixtures can me mixed in any proportion.

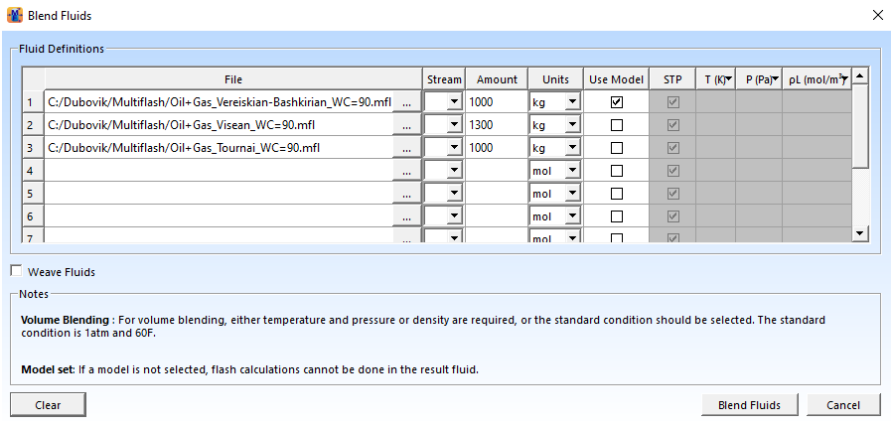

Figure 4.8: Composition of the Fluid-212

Hence, it was decided to use the Fluid-212 for further analysis, as its composition is similar to what is shown in Table 4.2 (Figure 4.8).

Then, properties of the Fluid-212 were studied at operational conditions of the oil-and-gas flowline from well cluster-7 to OTP 'Chernovskoe'. Operational conditions are shown in Table 3.1 ($P = 2.3$ MPa; $T = 20$ °C). To calculate properties of the Fluid-212 at constant pressure and temperature values, the PT Flash option in Multiflash was used (Table 4.6).

Table 4.6: Properties of the Fluid 212 at P=2.3 MPa, T=20 °C

Parameter	Unit	Value of parameter		
		Overall	**Liquid**	**Water**
Molecular weight		19.5237	27.7896	226.6210
Density	kg/m^3	967.4524	26.5639	892.3609
Viscosity	Pa·s	not defined	1.6885E-5	0.0102
C_p	J/(mol·K)	75.5987	32.2701	379.3456
C_v	J/(mol·K)	73.0486	22.6941	347.5338
Compressibility	1/MPa	0.0003	0.4394	0.0008
Expansivity	1/°C	0.0003	0.0037	0.0006
JT Coefficient	°C/MPa	-0.2290	2.7848	-0.5542
Sound speed	m/s	386.5534	349.0174	1231.3166

In order to use the Fluid-212 for further analysis, it was exported to tab-file (.tab), which is a set of PVT tables. PVT tables include the following data:

- gas, oil, water heat capacity tables;
- derivative of gas, oil, water density wrt pressure and wrt temperature tables;
- gas, oil, water enthalpy tables;
- gas, oil, water entropy tables;
- gas, oil, water thermal conductivity tables;
- gas, oil, water density tables;
- gas, oil, water viscosity tables;
- gas and water vapour mass fraction tables;
- gas/oil, gas/water, oil/water surface tension tables.

As an example, there are two PVT tables for the Fluid-212 shown in Figures 4.9-4.10.

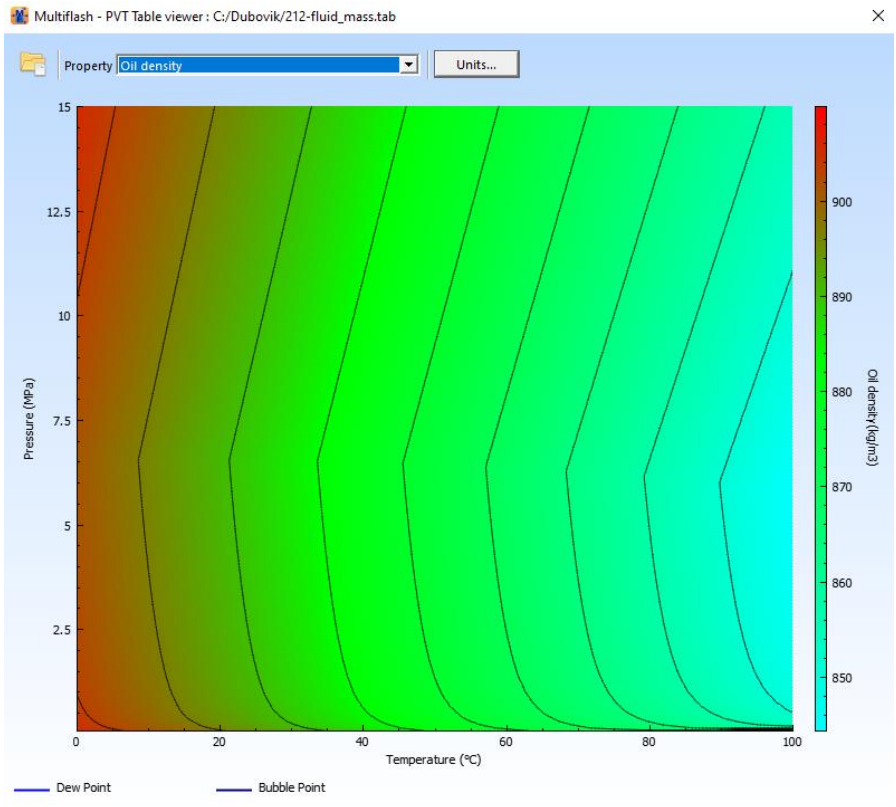

Figure 4.9: PVT table for the Fluid-212 – oil density

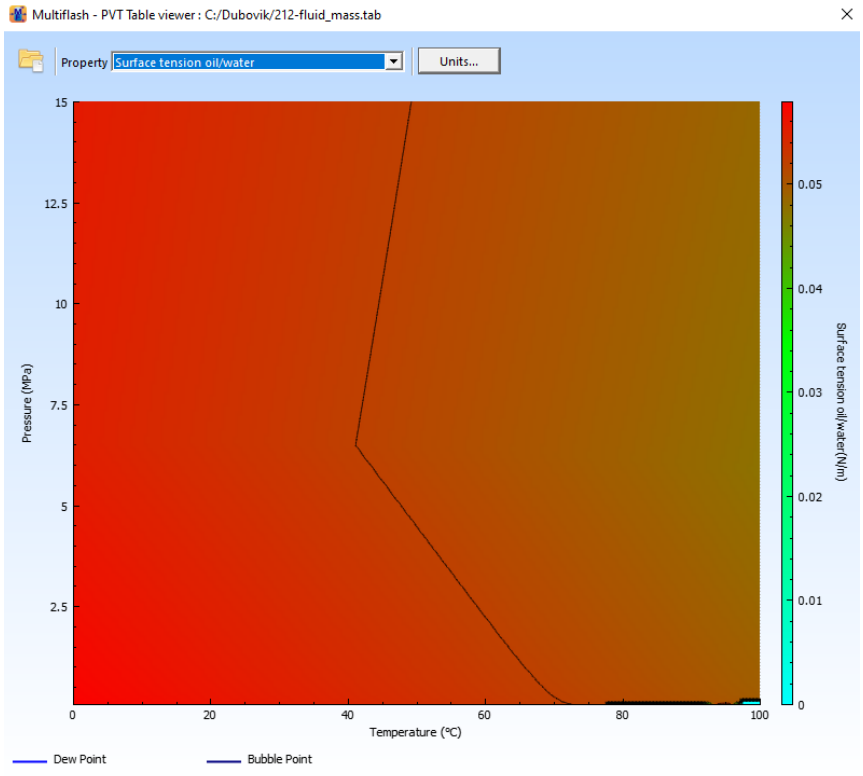

Figure 4.10: PVT table for the Fluid-212 – surface tension oil/water

4.2 Calculations in OLGA

Hydrodynamic properties of the unstable oil-and-gas emulsion in the oil-and-gas flowline were studied in OLGA dynamic multiphase flow simulator.

The first step was to create a flowpath. It had to be done using the data on the oil-and-gas flowline from well cluster-7 to OTP 'Chernovskoe' in accordance with Table 3.1 and Figure 3.1. The Pipeline Editor option in OLGA was used to set a route profile, segments, wall thickness, pipe length, diameter, material, coating, laying depth and ambient parameters. Also, the following discretization was set to conduct an accurate analysis – minimal section length of 5 m, maximum section length of 100 m and minimal amount of sections per pipe of 4 (Figure 4.11 and Tables 4.7-4.9).

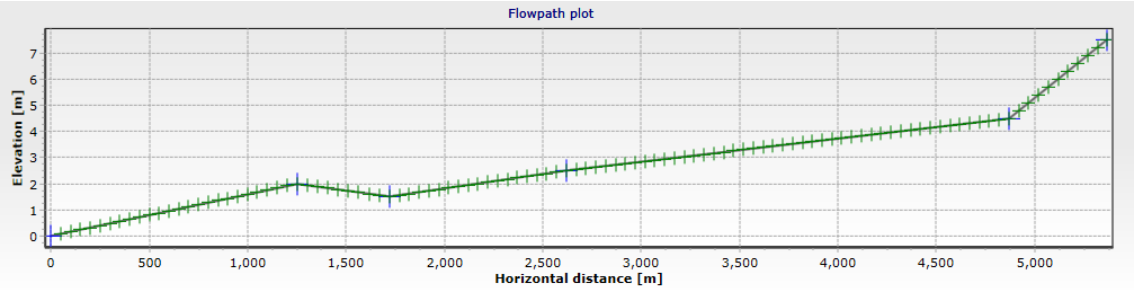

Figure 4.11: Flowpath plot

Table 4.7: Flowpath layout

Pipe number	Label	Diameter	Roughness	Length	Elevation	Wall
1 - 1	PIPE-3030	103 mm	0.05 mm	1250 m	2 m	WALL_3030
1 - 2	PIPE-3032	103 mm	0.05 mm	470 m	-0.5 m	WALL_3032
1 - 3	PIPE-3033	147 mm	0.05 mm	900 m	1 m	WALL_3033
1 - 4	PIPE-3035	147 mm	0.05 mm	2250 m	2 m	WALL_3035
1 - 5	PIPE-3037	147 mm	0.05 mm	500 m	3 m	WALL_3037

Table 4.8: Flowpath materials

Label	Density	Conductivity	Heat Capacity
Stainless Steel	7850 kg/m^3	20 W/m-C	450 J/(kg-C)
Bitumen Enamel	1325 kg/m^3	0.7 W/m-C	1300 J/(kg-C)
Soil	1750 kg/m^3	2.146 W/m-C	1031 J/(kg-C)

Table 4.9: Flowpath walls, coating and laying depth

Label	Material	Thickness	Elastic
	Stainless Steel	5.5 mm	OFF
WALL_3030	Bitumen Enamel	2 mm	
	Soil	1500 mm	
	Stainless Steel	5.5 mm	OFF
WALL_3032	Bitumen Enamel	2 mm	
	Soil	1500 mm	
	Stainless Steel	6 mm	OFF
WALL_3033	Bitumen Enamel	2 mm	
	Soil	1500 mm	
	Stainless Steel	6 mm	OFF
WALL_3035	Bitumen Enamel	2 mm	
	Soil	1500 mm	
	Stainless Steel	6 mm	OFF
WALL_3037	Bitumen Enamel	2 mm	
	Soil	1500 mm	

The second step was to import a tab-file for the Fluid-212 to OLGA. The Model Browser in OLGA was used to fulfill this task. Later, extra equipment had to be added – inlet, outlet, two valves and a massflow source (Figure 4.12).

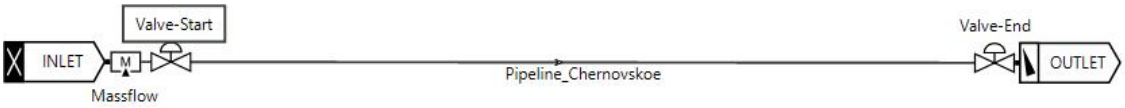

Figure 4.12: Flowpath sketch

The third step was to set boundary conditions – outlet pressure of 2.3 MPa, outlet temperature of 20 °C in accordance with data from Table 3.1.

Also, the mass flowrate had to be set. To do this, the data on actual volumetric flowrate was taken from Table 3.1 (Q = 3824 m^3/d) and density of the Fluid-212 from Table 4.6 (ρ = 967.4524 kg/m^3). Mass flowrate can be calculated as shown in equation (4.1):

$$Q_m = Q \cdot \rho \tag{4.1}$$

where Q_m is the mass flowrate (kg/d); Q is the volumetric flowrate (m^3/d); ρ is the density (kg/m^3).

Thus, the mass flowrate Q_m = 3699537.98 kg/d = 42.8187 kg/s.

The last step was to verify the model and run the simulation for 72 hours. The Run Batch option in OLGA was used for this purpose. When the simulation finished, desired output parameters had to be set up by choosing them from the range of available variables (Table 4.10).

Table 4.10: Desired output parameters

Parameter	Unit	Variable in OLGA
Representation of geometry	m	Geometry
Pressure	MPa	PT
Fluid temperature	°C	TM
Gas mass flowrate	kg/s	GG
Mass flowrate of oil	kg/s	GLTHL
Total mass flowrate of water including vapour	kg/s	GLWVT
Total mass flowrate	kg/s	GT
Gas volume flowrate	m^3/d	QG
Volumetric flowrate oil	m^3/d	QLTHL
Volumetric flowrate water	m^3/d	QLTWT
Total volume flowrate	m^3/d	QT
Flow regime (1 = stratified, 2 = annular, 3 = slug, 4 = bubble)		ID
Holdup (liquid volume fraction including solids)		HOL

The Profile Plot option in OLGA was used to plot diagrams which show magnitudes of desired parameters along the flowpath (Figures 4.13-4.16).

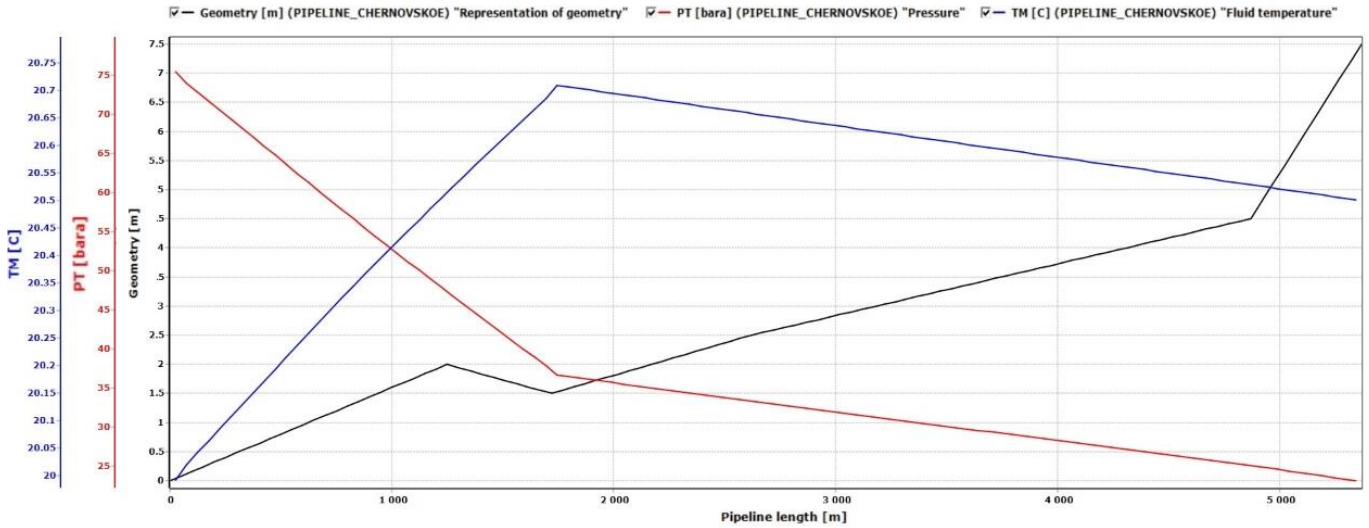

Figure 4.13: Geometry, pressure and temperature along the flowpath

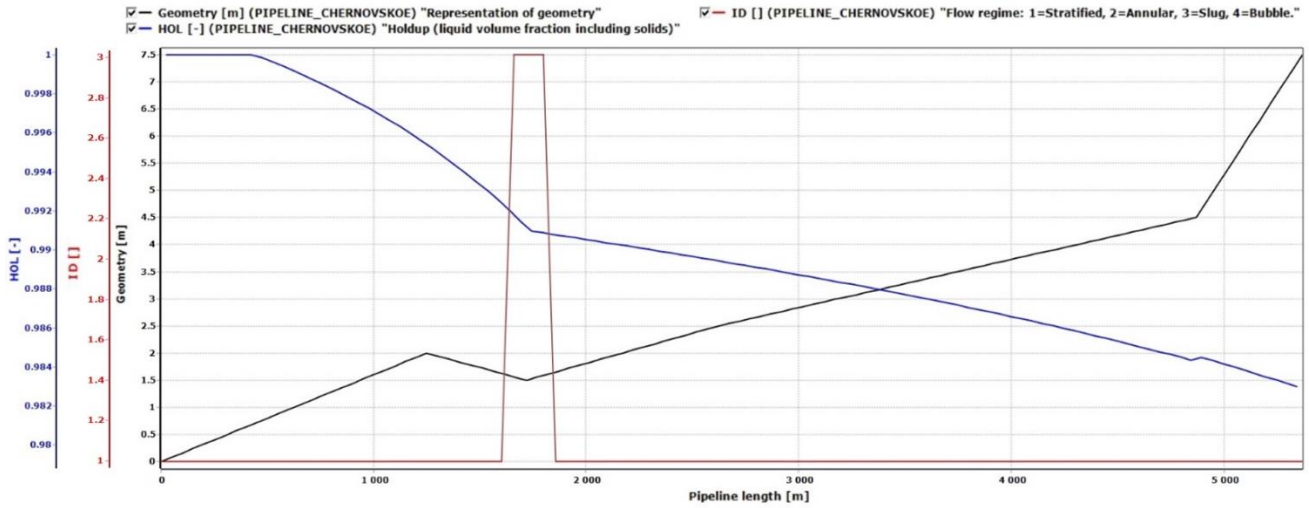

Figure 4.14: Geometry, flow regime and holdup along the flowpath

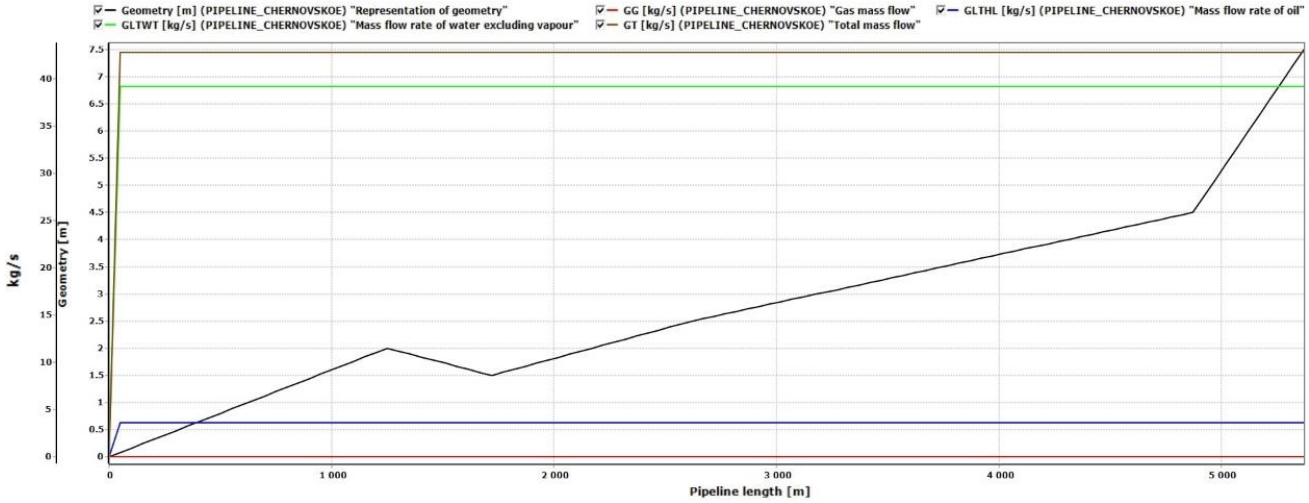

Figure 4.15: Geometry and mass flowrates along the flowpath

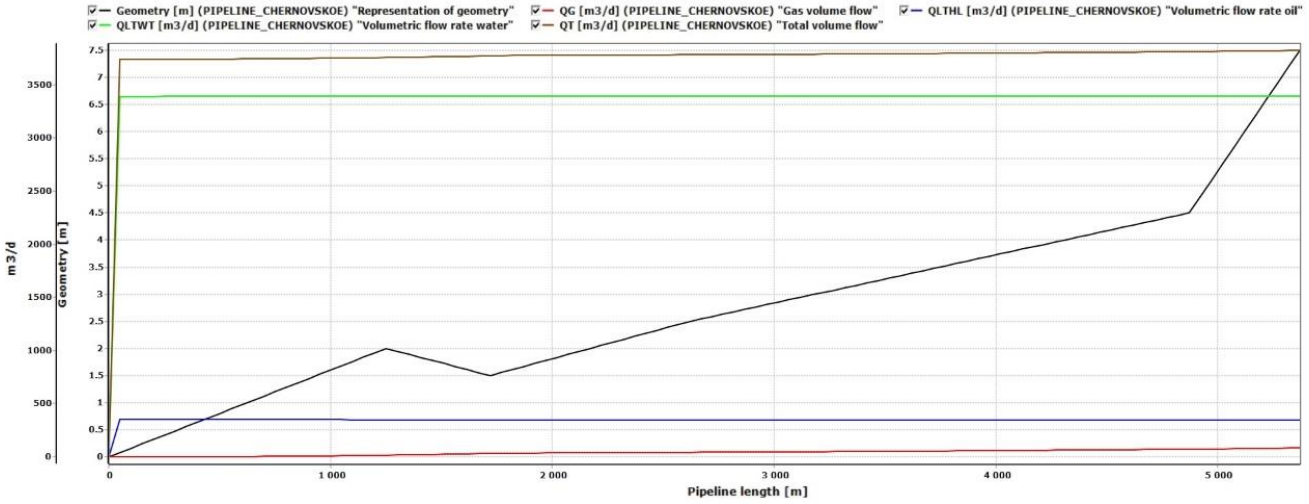

Figure 4.16: Geometry and volumetric flowrates along the flowpath

Eventually, the data from plots shown in Figures 4.13-4.16 had to be discussed:

- Figure 4.13 – a significant pressure gradient change is spotted in junction of Sections 3032 and 3033 of the flowpath. Temperature fluctuations are uneven.
- Figure 4.14 – the flow regime is mostly stratified, which is a positive factor. However, slug regime is spotted in junction of Sections 3032 and 3033 of the flowpath. Holdup changes slightly, but the fastest decline occurs in Sections 3030 and 3032 of the flowpath;
- Figure 4.15 – mass flowrates for all phases are constant;
- Figure 4.16 – volumetric flowrates are stable, without sharp fluctuations. Uneven growth in volumetric flowrate of gas and total volumetric flowrate is also spotted in junction of Sections 3032 and 3033 of the flowpath.

In accordance with the results, flow in the oil-and-gas flowline is characterized as unstable. The pipe inner diameter increase in junction of Sections 3032 and 3033 from 103 mm to 147 mm is assumed to be the main reason causing this phenomenon.

4.3 Calculations in PIPESIM

The PIPESIM simulator was used to study corrosion processes of unstable flow in the oil-and-gas flowline.

To begin with, a .mfl file for the Fluid-212 had to be imported to PIPESIM using the Fluid Manager. Then, two separate pipelines of different diameters were simulated, representing the the oil-and-gas flowline from well cluster-7 to OTP ‘Chernovskoe’. The input data is taken from Table 3.1, Figure 3.1 and Figures 4.13-4.16:

- Section 3030 and Section 3032 – L = 1720 m; T = 20 °C, inlet pressure of 7.7 MPa, outlet pressure of 3.71 MPa, elevation of 1.5 m, inner diameter of 103 mm, wall thickness of 5.5 mm; pH = 6, Q_m = 42.8187 kg/s;
- Section 3033, Section 3035 and Section 3037 – L = 3650 m; T = 20 °C, inlet pressure of 3.71 MPa, outlet pressure of 2.3 MPa, elevation of 6 m, inner diameter of 147 mm, wall thickness of 6 mm; pH = 6, Q_m = 42.8187 kg/s.

Finally, the de Waard corrosion model was applied. The Network Simulation option in PIPESIM was used to perform the analysis (Table 4.11). According to the data from Table 4.11, a plot was generated (Figure 4.17).

It is shown in Figure 4.17 that corrosion rate in very unstable and has high magnitudes in Section 3030 and Section 3032. However, corrosion rate significantly decreases and stabilizes in Section 3033, Section 3035 and Section 3037.

Table 4.11: Calculations in PIPESIM using the de Waard corrosion model

Total distance	Pressure, MPa	Fluid mean velocity, m/s	Corrosion rate, mm/year
0	7.7	4.9342	1.418817
344	6.412	4.9415	1.347667
688	5.939	4.9643	1.648195
1032	5.191	4.9958	1.197345
1376	4.373	5.0562	1.392222
1720	3.71	2.5587	0.4778
1903	3.643	2.5647	0.4715
2086	3.576	2.5708	0.4650
2269	3.508	2.5770	0.4584
2452	3.440	2.5832	0.4516
2635	3.372	2.5895	0.4448
2818	3.303	2.5959	0.4379
3001	3.233	2.6029	0.4308
3184	3.163	2.6114	0.4239
3367	3.092	2.6200	0.4167
3550	3.021	2.6287	0.4095
3733	2.949	2.6376	0.4020
3916	2.876	2.6466	0.3944
4099	2.802	2.6573	0.3868
4282	2.728	2.6693	0.3791
4465	2.653	2.6816	0.3712
4648	2.576	2.6941	0.3631
4831	2.499	2.7069	0.3548
5014	2.421	2.7231	0.3465
5197	2.841	2.7403	0.3380
5370	2.3	2.7580	0.3291

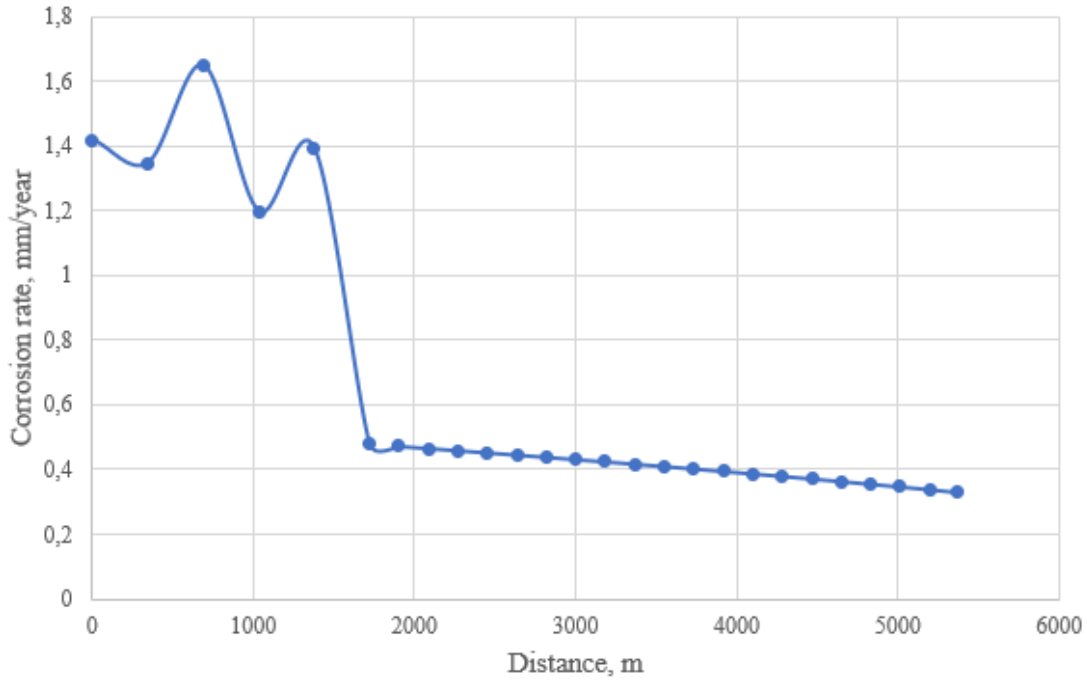

Figure 4.17: Corrosion rate calculated in PIPESIM

Chapter 5

Testing of corrosion inhibitors on the reservoir water model

5.1 Creation of the reservoir water model

With the purpose of obtaining the most accurate data on corrosion rate and efficiency of corrosion inhibitors in the oil-and-gas flowline from well cluster-7 to OTP 'Chernovskoe', it was decided to conduct a laboratory analysis of CO_2 corrosion.

In order to conduct the CO_2 corrosion experiment, a model of the fluid in the oil-and-gas flowline had to be created. The fluid is classified as the highly-aggressive unstable oil-in-water emulsion with solid particles and corrosion products in it. As there is no possibility to recreate exactly the same fluid, it was decided to make up a reservoir water model. Anyway, in accordance with data from Tables 3.2-3.5, water cut is higher than 90 wt. % and CO_2 fraction in composition of the fluid is sufficient. Moreover, previously completed calculations in software did not take a specific water composition into account.

Table 5.1: Chemical analysis of water on 21.04.2021 (sample from Section 3033)

Parameter	Unit	Value of parameter
Water density	kg/m^3	1180
HCO_3^- per volume	ppm	64.1
Cl^- per volume	ppm	171110
SO_4^{2-} per volume	ppm	511.1
Ca^{2+} per volume	ppm	17635.2
Mg^{2+} per volume	ppm	6000
Na^+ and K^+ per volume	ppm	82840.8

To begin with, the data on chemical analysis of water sample from Section 3033 (Table 3.6) was copied into Table 5.1.

A distilled water and five salts of analytic grade were used to create the reservoir water model:

- sodium bicarbonate ($NaHCO_3$);
- sodium sulfate (Na_2SO_4);
- calcium chloride dehydrate ($CaCl_2$);
- magnesium chloride hexahydrate ($MgCl_2 \cdot 6H_2O$);
- sodium chloride (NaCl).

To reveal the mass of each salt to be added into a distilled water, the molecular weight of each salt has to be defined (5.1). Then, the mass of each component of salt is calculated as shown in (5.2-5.3).

$$M(X_xY_y) = x \cdot M(X) + y \cdot M(Y) \tag{5.1}$$

where $M(X_xY_y)$ is the molecular weight of the mixture X_xY_y; $M(X)$ is the molecular weight of the element X; $M(Y)$ is the molecular weight of the element Y; x is the number of molecules of the element X; y is the number of molecules of the element Y.

$$m_{salt} = \frac{M_{salt} \cdot m_{comp}}{M_{comp}} \tag{5.2}$$

$$m_{comp} = \frac{M_{comp} \cdot m_{salt}}{M_{salt}} \tag{5.3}$$

where M_{comp} is the molecular weight of a component; M_{salt} is the molecular weight of a salt; m_{comp} is the mass of a component per 1 liter of a solution (g/L); m_{salt} is the mass of a salt per 1 liter of a solution (g/L).

Calculations for salts:

- sodium bicarbonate ($NaHCO_3$):
  a. $M_{HCO_3^-} = 1 + 12 + 3 \cdot 16 = 61$;
  b. $M_{NaHCO_3} = 23 + 61 = 84$;
  c. $m_{HCO_3} = 64.1 \cdot 10^{-3} = 0.0641$ g/L;
  d. $m_{NaHCO_3} = \frac{84 \cdot 0.0641}{61} = 0.0883$ g/L;
  e. $m_{Na^+} = \frac{23 \cdot 0.0883}{84} = 0.0242$ g/L;
- sodium sulfate (Na_2SO_4):
  a. $M_{SO_4^{2-}} = 32 + 4 \cdot 16 = 96$;
  b. $M_{Na_2SO_4} = 2 \cdot 23 + 96 = 142$;

c. $m_{SO_4^{2-}} = 511.1 \cdot 10^{-3} = 0.5111$ g/L;

d. $m_{Na_2SO_4} = \frac{142 \cdot 0.5111}{96} = 0.756$ g/L;

e. $m_{Na^+} = \frac{23 \cdot 0.0883}{84} = 0.2449$ g/L;

- calcium chloride dehydrate ($CaCl_2$):

a. $M_{Cl_2^-} = 2 \cdot 35.5 = 71$;

b. $M_{CaCl_2} = 40 + 71 = 111$;

c. $m_{Ca^{2+}} = 17635.2 \cdot 10^{-3} = 17.6352$ g/L;

d. $m_{CaCl_2} = \frac{111 \cdot 17.6352}{40} = 48.9377$ g/L;

e. $m_{Cl^-} = \frac{71 \cdot 48.9377}{111} = 31.3025$ g/L;

- magnesium chloride hexahydrate ($MgCl_2 \cdot 6H_2O$):

a. $M_{MgCl_2} = 24 + 35.5 = 94$;

b. $M_{MgCl_2 \cdot 6H_2O} = 94 + 6 \cdot (2 \cdot 1 + 16) = 94 + 6 \cdot 18 = 202$;

c. $m_{Mg^{2+}} = 6000 \cdot 10^{-3} = 6$ g/L;

d. $m_{MgCl_2 \cdot 6H_2O} = \frac{202 \cdot 6}{24} = 50.5$ g/L;

e. $m_{MgCl_2} = \frac{94 \cdot 50.5}{202} = 23.5$ g/L;

f. $m_{Cl^-} = \frac{71 \cdot 23.5}{94} = 17.75$ g/L;

- sodium chloride (NaCl):

a. $M_{NaCl} = 23 + 35.5 = 58.5$;

b. $m_{Cl^-}(\text{total}) = 171110 \cdot 10^{-3} = 171.110$ g/L;

c. $m_{Cl^-}(\text{to be added}) = 171.110 - 17.75 - 31.3025 = 122.0575$ g/L;

d. $m_{NaCl} = \frac{58.5 \cdot 122.0575}{35.5} = 201.137$ g/L;

e. $m_{Na^+} = \frac{23 \cdot 201.137}{58.5} = 79.0795$ g/L;

- residual K^+:

a. $m_{Na^+ + K^+} = 82.8408$ g/L;

b. $m_{K^+} = m_{Na^+ + K^+} - m_{Na^+} = 82.8408 - (79.0795 + 0.2449 + 0.0242) = 3.4922$ g/L;

It was decided to neglect the presence of K^+ in the reservoir water model. Thus, according to the calculations above, the following mass of salts had to be dissolved per 1 liter of the the reservoir water model:

- sodium bicarbonate ($NaHCO_3$) – 0.064 g;
- sodium sulfate (Na_2SO_4) – 0.756 g;
- calcium chloride dehydrate ($CaCl_2$) – 48.9377 g;

- magnesium chloride hexahydrate ($MgCl_2 \cdot 6H_2O$) – 50.5 g;
- sodium chloride (NaCl) – 201.137 g.

In order to obtain better quality of the reservoir water model, water solution had to be mixed only per 0.5 liter. Consequently, the mass of salts dissolved per 0.5 liter of the reservoir water model:

- sodium bicarbonate ($NaHCO_3$) – 0.038 g ≈ 0.04 g;
- sodium sulfate (Na_2SO_4) – 0.378 g ≈ 0.38 g;
- calcium chloride dehydrate ($CaCl_2$) – 24.4689 g ≈ 24.47 g;
- magnesium chloride hexahydrate ($MgCl_2 \cdot 6H_2O$) = 25.25 g;
- sodium chloride (NaCl) – 100.5685 ≈ 100.57 g.

The desired mass of salt had to be it taken from a jar by means of a spoon and weighed on the analytical scales A&D EK-200i with a measurement error of 0.01 g (Figures 5.1-5.6).

Figure 5.1: Salts used to create the reservoir water model

Figure 5.2: Salt weighing – sodium bicarbonate ($NaHCO_3$)

Figure 5.3: Salt weighing – sodium sulfate (Na_2SO_4)

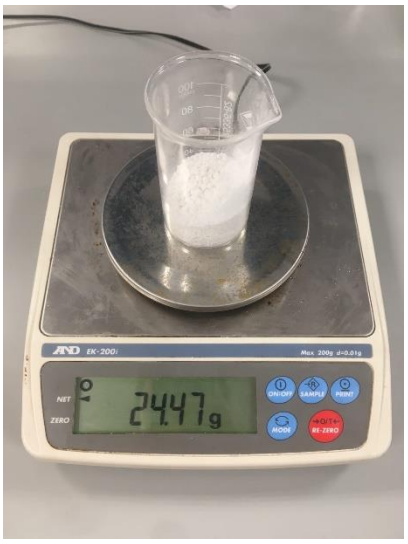

Figure 5.4: Salt weighing – calcium chloride dehydrate ($CaCl_2$)

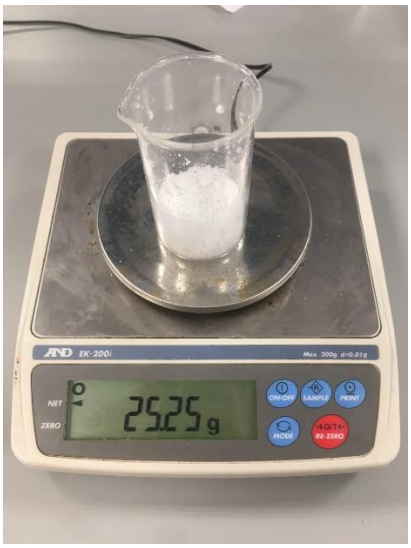

Figure 5.5: Salt weighing – magnesium chloride hexahydrate ($MgCl_2 \cdot 6H_2O$)

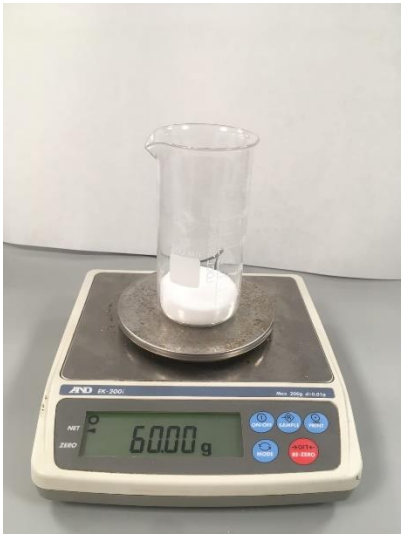

Figure 5.6: Salt weighing – sodium chloride (NaCl)

At the next step a glass cylinder and a magnetic stirrer MS300 with a magnetic anchor were used for mixing purposes, providing an ability to move particles in a solution intensively, saturating a distilled water with added salts (Figure 5.7). The mixing process lasted at least 20 minutes. A process of salt dissolution is exothermic. Therefore, a glass cylinder became warm.

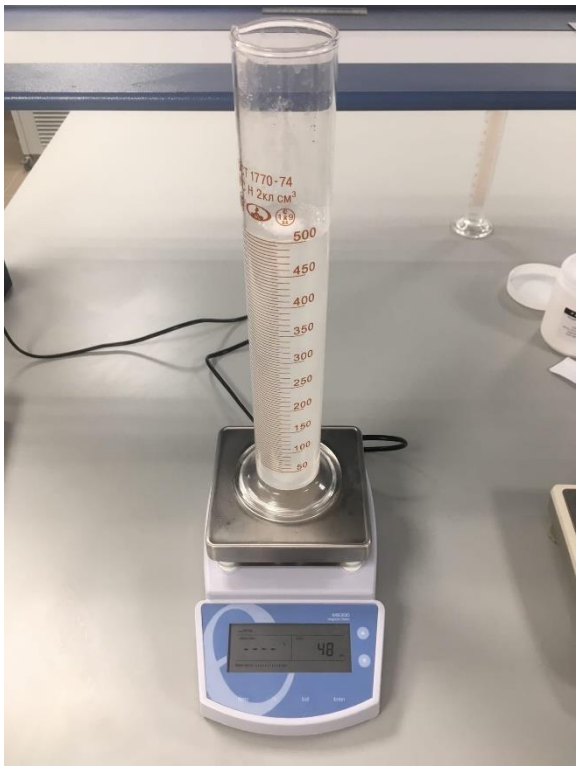

Figure 5.7: Creation of the reservoir water model by means of a glass cylinder and a magnetic stirrer MS300

When the reservoir water model was created, some sediments still remained and the water solution was cloudy and milky. The water solution had to be filtered by means of a filter paper,

a funnel and one more glass cylinder (Figure 5.8). The main objective of this procedure is to remove undissolved salt particles. After filtering, the water solution became transparent.

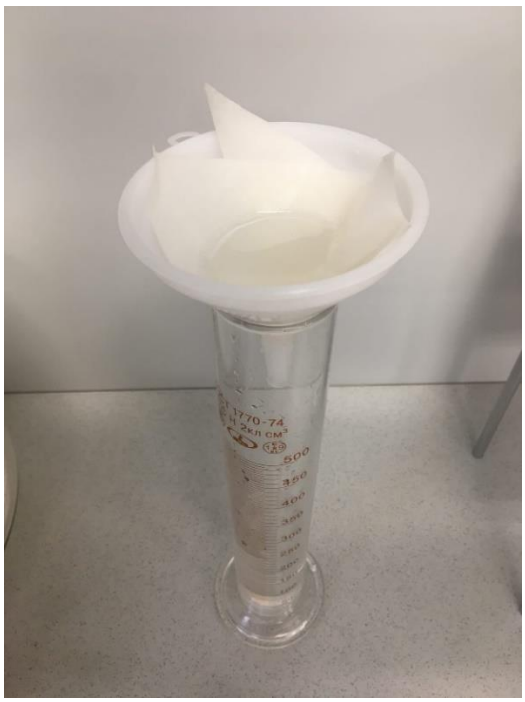

Figure 5.8: Filtering process

The next step was to measure the density of the reservoir water model. The areometer AON-1 and a glass cylinder were used for this purpose (Figure 5.9). The measured density equals 1180 kg/m^3, which correlates with data in Table 5.1. The reservoir water model was created successfully.

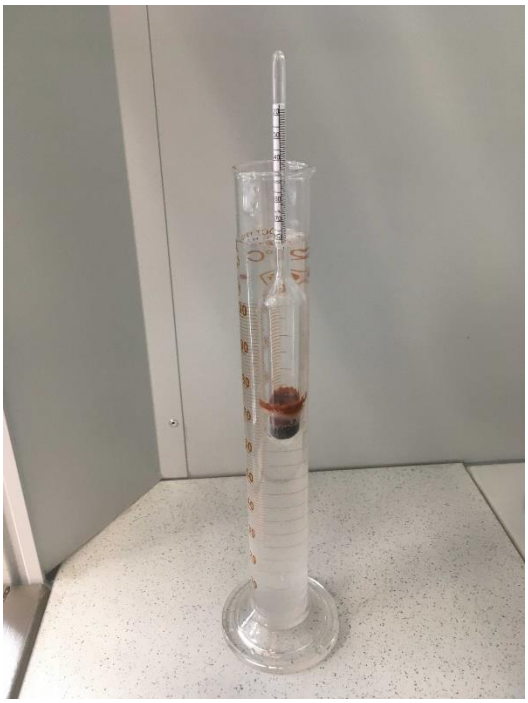

Figure 5.9: Measuring a density by means of the aerometer AON-1

It was decided to study four different reservoir water models in this Thesis to carry out an accurate analysis. Models have the same composition, but differ in densities and dissolved sodium chloride (NaCl) mass per 0.5 liter of the reservoir water model:

- ρ = 1114 kg/m^3, m_{NaCl} = 40 g;
- ρ = 1137 kg/m^3, m_{NaCl} = 60 g;
- ρ = 1160 kg/m^3, m_{NaCl} = 80 g;
- ρ = 1180 kg/m^3, m_{NaCl} = 100.57 g.

Moreover, each reservoir water model was examined under influence of three different corrosion inhibitors:

- SNPH-6418B (Figure 5.10);
- SONKOR-9020 (Figure 5.11);
- FLEK-IK-200 (Figure 5.12).

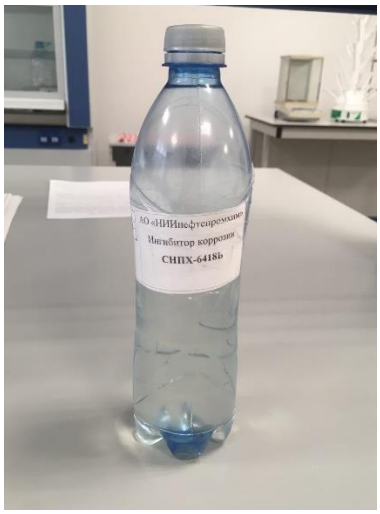

Figure 5.10: Corrosion inhibitor SNPH-6418B

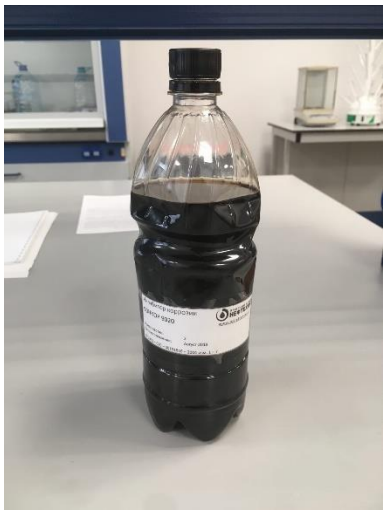

Figure 5.11: Corrosion inhibitor SONKOR-9020

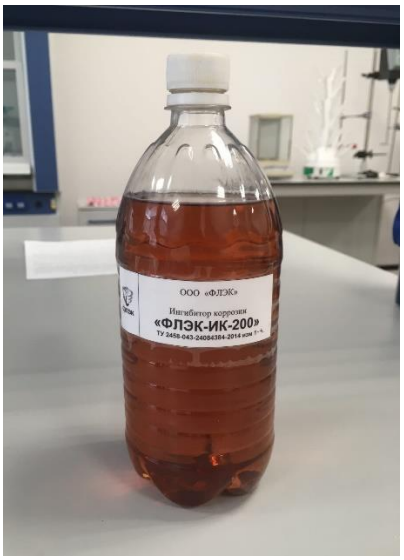

Figure 5.12: Corrosion inhibitor FLEK-IK-200

5.2 Methodology for corrosion inhibitors testing in CO_2 media

Corrosion inhibitors are tested in accordance with the normative documents (GOST 9.905-82, 1983); (GOST 9.502-82, 1984); (GOST 9.506-87, 1988). The corrosive aggressiveness of media is assessed by the gravimetric method.

The method consists in determining the mass loss of metal samples during their stay in inhibited and non-inhibited test media, followed by an assessment of the protective ability of the inhibitor by differences in corrosion rate magnitudes.

For testing, six flat samples made of steel St 20 with dimensions of 4.0 x 1.0 x 0.15 cm are used (Figure 5.13)

Figure 5.13: Flat metal samples made of steel St 20 before the experiment

Preparation of metal samples for testing is carried out as follows:

- each metal sample is degreased with acetone (Figure 5.14);
- metal samples are immersed in a hydrochloric acid solution (HCl 15%) for 1 minute to activate the surface before testing (Figure 5.15);
- each metal sample is thoroughly washed with running and distilled water (Figure 5.16);
- each metal sample is dried with filter paper, wrapped in it, and put in a desiccator with a desiccant inside of it for 1 hour (Figure 5.17);
- after 1 hour, each metal sample is weighed on high-precise analytical scales, such as A&D HR-250AZG with a measurement error of 0.0001 g (Figure 5.18).

Figure 5.14: Metal samples in acetone

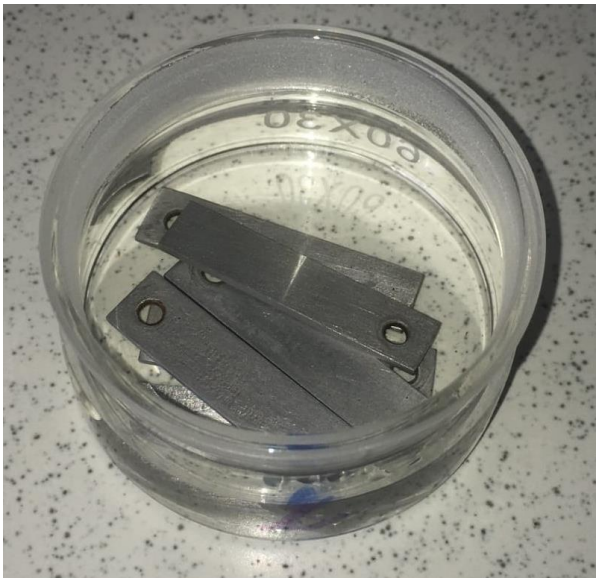

Figure 5.15: Metal samples in hydrochloric acid solution (HCl 15%)

Figure 5.16: Running and distilled water in vessels

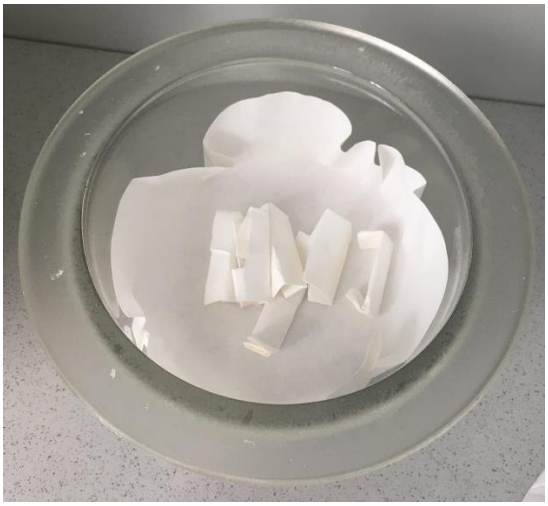

Figure 5.17: Metal samples (wrapped in filter paper) in a desiccator

Figure 5.18: Metal sample on the high-precise analytical scales A&D HR-250AZG

A vessel filled with the reservoir water model without inhibitor serves as a control sample. Another vessel is filled with the reservoir water model too, but with an inhibitor injected (Figure 5.19).

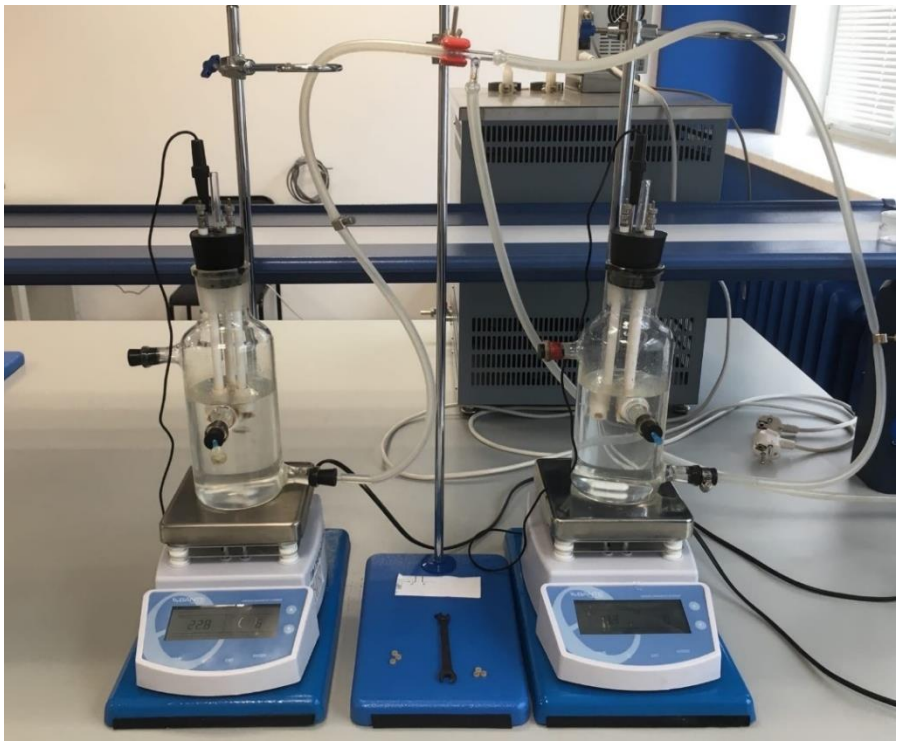

Figure 5.19: The experimental unit

For corrosion inhibitors dispensing, the pipette dispenser 'Lite' is used. It is capable of withdrawing liquids in a volume of 5-50 µL (Figure 5.20).

Figure 5.20: The pipette dispenser 'Lite'

The process of corrosion inhibitors testing is as follows:

- 600 cm^3 of the liquid is poured into two similar vessels made of glass;
- the vessels are mounted on magnetic stirrers;
- the liquid in the vessels is saturated with carbon dioxide by bubbling at atmospheric pressure for 1 hour (Figure 5.21);
- magnetic stirrers are turned on, intensively mixing the liquid in the vessels for 1 hour;
- after 1 hour, three prepared metal samples are placed into each vessel (Figure 5.22);

- a calculated amount of a corrosion inhibitor by means of equation (5.4) is injected into one of the vessels using the pipette dispenser ‘Lite’ (Figure 5.23);
- magnetic stirrers are turned on, intensively mixing the liquid in the vessels for 5 hours at 25 °C (Figure 5.24);
- after 5 hours, metal samples are removed from the vessels (Figure 5.25), washed with running and distilled water, and then dried with filter paper;
- metal samples are intensively wiped with an eraser. This procedure is required to clean the surface of metal samples by removing a film of corrosion products;
- metal samples are degreased with acetone and put in a desiccator for 1 hour;
- after 1 hour, each metal sample is weighed on highly-precise analytical scales. A measurement error of scales used for this procedure must not exceed 0.0001 gramm;
- calculation of the corrosion rate.

Figure 5.21: A CO_2 tank connected to the experimental unit

Figure 5.22: Metal samples attached to the experimental unit

Figure 5.23: The pipette dispenser 'Lite' in operation

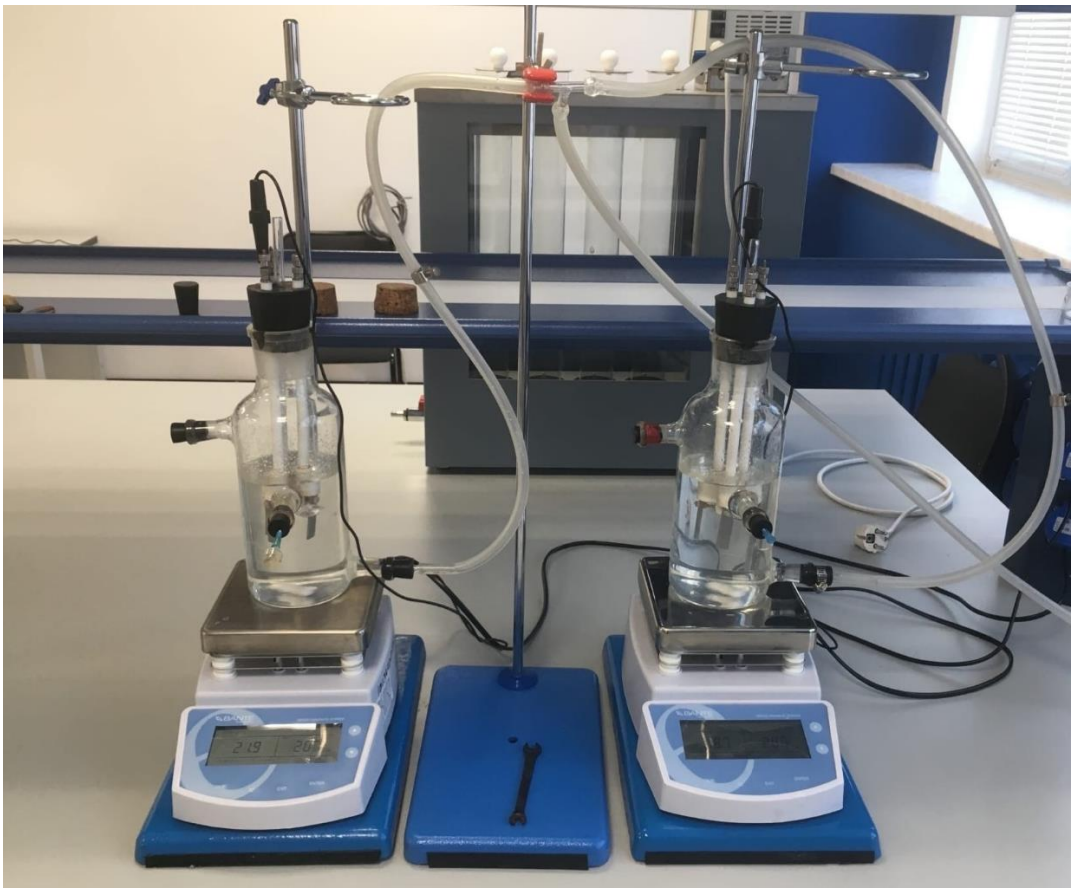

Figure 5.24: The experimental unit in operation with metal samples attached

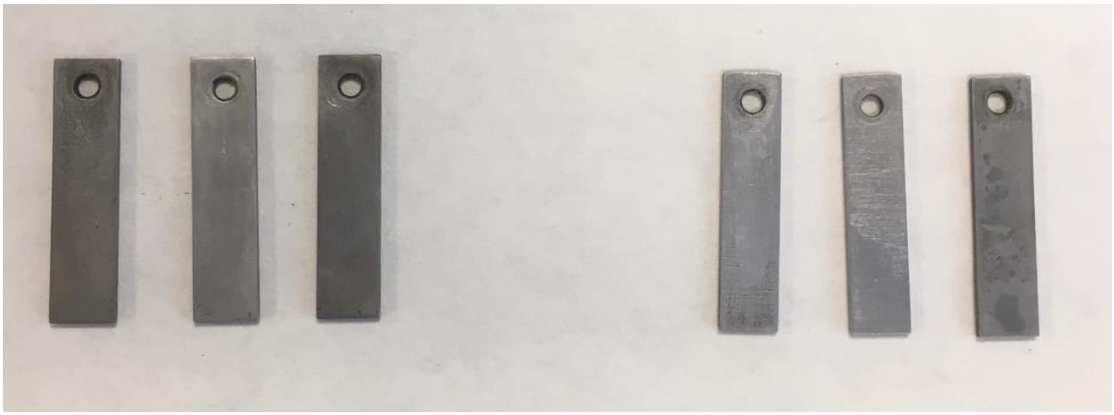

Figure 5.25: Flat metal samples made of steel St 20 after the experiment. No inhibitor (left), inhibitor injected (right)

Metal samples after each experiment looked almost similar – the presence of oxide film was spotted, which is a corrosion product. It was impossible to define whether samples were located in inhibited or not inhibited media without weighing.

The amount of a corrosion inhibitor to be injected is calculated using the equation (5.4):

$$w_{inh} = \frac{m_{inh} \cdot w_{fluid}}{\rho_{inh}} \cdot 10^6 \tag{5.4}$$

where w_{inh} is the amount of a corrosion inhibitor to be injected (μL); m_{inh} is the mass of a corrosion inhibitor per 1 liter of a solution (g/L); w_{fluid} is the volume of a solution (L); ρ_{inh} is the density of a corrosion inhibitor (kg/m^3).

The mass of a corrosion inhibitor per 1 liter of a solution is usually defined by the rule of thumb. In this analysis, it was defined as 30 mg/L or 0.03 g/L for each corrosion inhibitor. Calculations of corrosion inhibitors by means of equation (5.4) are shown in Table 5.2.

Table 5.2: Calculations of corrosion inhibitors

Corrosion inhibitor	ρ_{inh}, **kg/m^3**	m_{inh}, **g/L**	w_{inh}, **μL**
SNPH-6418B	931	0.03	19.33
SONKOR-9020	919	0.03	19.59
FLEK-IK-200	878	0.03	20.5

The corrosion rate for each metal sample is calculated as shown in equation (5.5):

$$V_C = \frac{m_1 - m_2}{A \cdot t} \tag{5.5}$$

where V_C is the corrosion rate (g/[m^2·h]); m_1 is the mass of a metal sample before the experiment (g); m_2 is the mass of a metal sample after the experiment (g); A is the surface area of a metal sample (m^2), t is the duration of the experiment (h).

The corrosion rate (penetration) is calculated as shown in equation (5.6):

$$V_{CP} = 1.12 \cdot V_C \tag{5.6}$$

where V_{CP} is the corrosion rate (penetration) (mm/year).

The index of corrosion protection is calculated as shown in equation (5.7):

$$Z = \frac{V_{C0} - V_{Ci}}{V_{C0}} \cdot 100\% \tag{5.7}$$

where Z is the index of corrosion protection; V_{Co} is the corrosion rate without inhibitor (g/[m^2·h]); V_{Ci} is the corrosion rate with an inhibitor injected (g/[m^2·h]).

5.3 Calculations of corrosion rate

A series of calculations by means of equations (5.5-5.7) was performed when 12 experiments were finished. The results for every reservoir water model with every corrosion inhibitor are shown in Tables 5.3-5.14.

Based on data from Tables 5.3-5.14, the average corrosion rate (penetration) was defined for each reservoir water model (Table 5.15). Then, the plot was constructed (Figure 5.26).

All in all, 12 experiments were carried out. Each experiment required 1.2 liters of the reservoir water model. As each reservoir water model was tested under influence of three different corrosion inhibitors, 3.6 liters of each reservoir water model required. Taking losses during mixing, filtering, spilling and testing into account, it was decided to prepare 4 liters of each reservoir water model. Hence, almost 16 liters of a distilled water was used. Water solutions have been mixed 32 times. So, an impressive amount of salts was used:

- sodium bicarbonate ($NaHCO_3$) – 1.28 g;
- sodium sulfate (Na_2SO_4) – 12.16 g;
- calcium chloride dehydrate ($CaCl_2$) – 783.04 g;
- magnesium chloride hexahydrate ($MgCl_2 \cdot 6H_2O$) – 808 g;
- sodium chloride (NaCl) – 2244.56 g.

In general, each experiment lasted more than 7 hours. Thus, more than 84 hours were spent to carry out all 12 laboratory experiments devoted to testing of corrosion inhibitors on the reservoir water model.

Table 5.3: Calculations of corrosion rate at ρ=1114 kg/m³; SNPH-6418B

Media of solution	Sample number	Mass of a metal sample			Corrosion rate, g/(m²·h)	Average corrosion rate, g/(m²·h)	Corrosion rate (penetration), mm/year	Index of corrosion protection
		m_1, g	m_2, g	m_1-m_2, g				
Inhibitor SNPH-6418B	1	4.7140	4.7137	0.0003	0.0632			
	2	4.6591	4.6584	0.0007	0.1474	0.0982	0.1100	
	3	4.7807	4.7803	0.0004	0.0842			36.36
No inhibitor injected	4	3.9509	3.9503	0.0006	0.1263			
	5	3.9163	3.9157	0.0006	0.1263	0.1544	0.1729	
	6	3.7638	3.7628	0.0010	0.2105			

Table 5.4: Calculations of corrosion rate at ρ=1114 kg/m³; SONKOR-9020

Media of solution	Sample number	Mass of a metal sample			Corrosion rate, g/(m²·h)	Average corrosion rate, g/(m²·h)	Corrosion rate (penetration), mm/year	Index of corrosion protection
		m_1, g	m_2, g	m_1-m_2, g				
Inhibitor SONKOR-9020	1	4.6656	4.6646	0.0010	0.2105			
	2	4.7879	4.7871	0.0008	0.1684	0.2035	0.2279	
	3	4.7215	4.7204	0.0011	0.2316			3.33%
No inhibitor injected	4	3.9570	3.9560	0.0010	0.2105			
	5	3.9235	3.9227	0.0008	0.1684	0.2105	0.2358	
	6	3.7732	3.7720	0.0012	0.2526			

Table 5.5: Calculations of corrosion rate at ρ=1114 kg/m³; FLEK-IK-200

Media of solution	Sample number	Mass of a metal sample			Corrosion rate, g/(m²·h)	Average corrosion rate, g/(m²·h)	Corrosion rate (penetration), mm/year	Index of corrosion protection
		m_1, g	m_2, g	m_1-m_2, g				
Inhibitor FLEK-IK-200	1	4.7883	4.7879	0.0004	0.0842			
	2	4.7230	4.7227	0.0003	0.0632	0.0772	0.0865	
	3	4.6662	4.6658	0.0004	0.0842			-22.22%
No inhibitor injected	4	3.9238	3.9235	0.0003	0.0632			
	5	3.7740	3.7738	0.0002	0.0421	0.0632	0.0707	
	6	3.9574	3.9570	0.0004	0.0842			

Table 5.6: Calculations of corrosion rate at ρ=1137 kg/m³; SNPH-6418B

Media of solution	Sample number	Mass of a metal sample			Corrosion rate, g/(m²·h)	Average corrosion rate, g/(m²·h)	Corrosion rate (penetration), mm/year	Index of corrosion protection
		m_1, g	m_2, g	m_1-m_2, g				
Inhibitor SNPH-6418B	1	3.9547	3.9542	0.0005	0.1053			
	2	3.9204	3.9198	0.0006	0.1263	0.0842	0.0943	
	3	3.7690	3.7689	0.0001	0.0211			52%
No inhibitor injected	4	4.7862	4.7852	0.0010	0.2105			
	5	4.6633	4.6624	0.0009	0.1895	0.1754	0.1965	
	6	4.7182	4.7176	0.0006	0.1263			

Table 5.7: Calculations of corrosion rate at ρ=1137 kg/m³; SONKOR-9020

Media of solution	Sample number	Mass of a metal sample			Corrosion rate, g/(m²·h)	Average corrosion rate, g/(m²·h)	Corrosion rate (penetration), mm/year	Index of corrosion protection
		m_1, g	m_2, g	m_1-m_2, g				
Inhibitor SONKOR-9020	1	4.6612	4.6606	0.0006	0.1263			
	2	4.7163	4.7156	0.0007	0.1474	0.1474	0.1651	
	3	4.7831	4.7823	0.0008	0.1684			27.59%
No inhibitor injected	4	3.7672	3.7660	0.0012	0.2526			
	5	3.9186	3.9181	0.0005	0.1053	0.2035	0.2279	
	6	3.9535	3.9523	0.0012	0.2526			

Table 5.8: Calculations of corrosion rate at ρ=1137 kg/m³; FLEK-IK-200

Media of solution	Sample number	Mass of a metal sample			Corrosion rate, g/(m²·h)	Average corrosion rate, g/(m²·h)	Corrosion rate (penetration), mm/year	Index of corrosion protection
		m_1, g	m_2, g	m_1-m_2, g				
Inhibitor FLEK-IK-200	1	4.6635	4.6632	0.0003	0.0632			
	2	4.7865	4.7859	0.0006	0.1263	0.1193	0.1336	
	3	4.7192	4.7184	0.0008	0.1684			37.04%
No inhibitor injected	4	3.9217	3.9206	0.0011	0.2316			
	5	3.7703	3.7695	0.0008	0.1684	0.1895	0.2122	
	6	3.9555	3.9547	0.0008	0.1684			

Table 5.9: Calculations of corrosion rate at ρ=1160 kg/m³; SNPH-6418B

Media of solution	Sample number	Mass of a metal sample			Corrosion rate, g/(m²·h)	Average corrosion rate, g/(m²·h)	Corrosion rate (penetration), mm/year	Index of corrosion protection
		m_1, g	m_2, g	m_1-m_2, g				
Inhibitor SNPH-6418B	1	4.6801	4.6795	0.0006	0.1263			
	2	3.9660	3.9655	0.0005	0.1053	0.1193	0.1336	
	3	4.8012	4.8006	0.0006	0.1263			32%
No inhibitor injected	4	4.7369	4.7361	0.0008	0.1684			
	5	3.7886	3.7875	0.0011	0.2316	0.1754	0.1965	
	6	3.9344	3.9338	0.0006	0.1263			

Table 5.10: Calculations of corrosion rate at ρ=1160 kg/m³; SONKOR-9020

Media of solution	Sample number	Mass of a metal sample			Corrosion rate, g/(m²·h)	Average corrosion rate, g/(m²·h)	Corrosion rate (penetration), mm/year	Index of corrosion protection
		m_1, g	m_2, g	m_1-m_2, g				
Inhibitor SONKOR-9020	1	3.7779	3.7775	0.0004	0.0842			
	2	3.9264	3.9256	0.0008	0.1684	0.1404	0.1572	
	3	3.9591	3.9583	0.0008	0.1684			28.57%
No inhibitor injected	4	4.6706	4.6699	0.0007	0.1474			
	5	4.7916	4.7906	0.0010	0.2105	0.1965	0.2201	
	6	4.7266	4.7255	0.0011	0.2316			

Table 5.11: Calculations of corrosion rate at ρ=1160 kg/m³; FLEK-IK-200

Media of solution	Sample number	Mass of a metal sample			Corrosion rate, g/(m²·h)	Average corrosion rate, g/(m²·h)	Corrosion rate (penetration), mm/year	Index of corrosion protection
		m_1, g	m_2, g	m_1-m_2, g				
Inhibitor FLEK-IK-200	1	4.7869	4.7867	0.0002	0.0421			
	2	4.6644	4.6635	0.0009	0.1895	0.1193	0.1336	
	3	4.7204	4.7198	0.0006	0.1263			-6.25%
No inhibitor injected	4	3.9223	3.9217	0.0006	0.1263			
	5	3.9560	3.9555	0.0005	0.1053	0.1123	0.1258	
	6	3.7711	3.7706	0.0005	0.1053			

Table 5.12: Calculations of corrosion rate at ρ=1180 kg/m³; SNPH-6418B

Media of solution	Sample number	Mass of a metal sample			Corrosion rate, g/(m²·h)	Average corrosion rate, g/(m²·h)	Corrosion rate (penetration), mm/year	Index of corrosion protection
		m_1, g	m_2, g	m_1-m_2, g				
Inhibitor SNPH-6418B	1	4.7819	4.7817	0.0002	0.0421			
	2	4.6603	4.6596	0.0007	0.1474	0.0912	0.1022	
	3	4.7153	4.7149	0.0004	0.0842			40.91%
No inhibitor injected	4	3.9176	3.9171	0.0005	0.1053			
	5	3.7652	3.7644	0.0008	0.1684	0.1544	0.1729	
	6	3.9523	3.9514	0.0009	0.1895			

Table 5.13: Calculations of corrosion rate at ρ=1180 kg/m³; SONKOR-9020

Media of solution	Sample number	Mass of a metal sample			Corrosion rate, g/(m²·h)	Average corrosion rate, g/(m²·h)	Corrosion rate (penetration), mm/year	Index of corrosion protection
		m_1, g	m_2, g	m_1-m_2, g				
Inhibitor SONKOR-9020	1	3.9170	3.9163	0.0007	0.1474			
	2	3.9514	3.9509	0.0005	0.1053	0.1263	0.1415	
	3	3.7643	3.7637	0.0006	0.1263			25%
No inhibitor injected	4	4.6592	4.6589	0.0003	0.0632			
	5	4.7147	4.7139	0.0008	0.1684	0.1684	0.1886	
	6	4.7817	4.7804	0.0013	0.2737			

Table 5.14: Calculations of corrosion rate at ρ=1180 kg/m³; FLEK-IK-200

Media of solution	Sample number	Mass of a metal sample			Corrosion rate, g/(m²·h)	Average corrosion rate, g/(m²·h)	Corrosion rate (penetration), mm/year	Index of corrosion protection
		m_1, g	m_2, g	m_1-m_2, g				
Inhibitor FLEK-IK-200	1	4.6502	4.6497	0.0005	0.1053			
	2	4.7089	4.7082	0.0007	0.1474	0.1404	0.1572	
	3	4.7754	4.7746	0.0008	0.1684			4.76%
No inhibitor injected	4	3.9113	3.9106	0.0007	0.1474			
	5	3.9459	3.9451	0.0008	0.1684	0.1474	0.1651	
	6	3.7587	3.7581	0.0006	0.1263			

Table 5.15: Summarized data on corrosion rate calculations

Density, kg/m$_3$	Corrosion penetration rate, mm/year			
	No inhibitor (average)	SNPH-6418B	SONKOR-9020	FLEK-IK-200
1114	0.1598	0.1100	0.2279	0.0865
1137	0.2122	0.0943	0.1651	0.1336
1160	0.1808	0.1336	0.1572	0.1336
1180	0.1755	0.1022	0.1415	0.1572

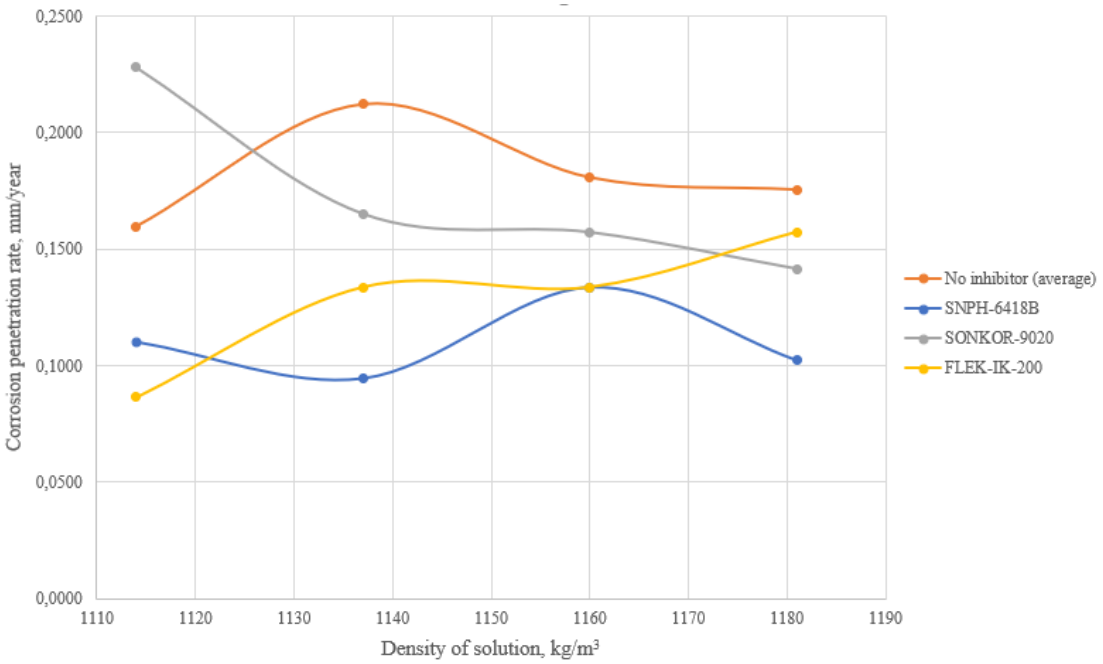

Figure 5.26: Corrosion rate at different reservoir water models under influence of different corrosion inhibitors in CO_2 media

On one hand, the most effective corrosion inhibitor at the reservoir water model ρ = 1180 kg/m^3 is SNPH-6418B, as it has the best index of corrosion protection of 40.91% and impressive performance over all the reservoir models tested.

On another hand, SONKOR-9020 is not stable enough, as it had bad performance at the reservoir water model ρ = 1114 kg/m^3. FLEK-IK-200 has an average performance.

The data on inhibitors tested should be verified by means of field testing of each inhibitor. Then, the data need to be compared with Table 3.8.

Chapter 6

Results and Discussion

6.1 Results of Chapter 2

Chapter 2 is devoted to a literature review of scientific articles and an analysis of existing mathematical models that can characterize a multiphase flow consisting of liquid and solid phases. The concept of multiphase systems is given and examples of existing multiphase systems are presented.

The evolution of liquid-solid two-phase flow models was demonstrated – from the simplest model, which does not take the influence of solid particles on properties of a flow into account (Tchen, 1947), to the very innovative one, which is able not only to consider the influence of solid particles on properties of a multiphase flow, but also takes growth and change of solid particles into account (Li, Li, Wang et al., 2020).

A deep analysis of each presented model was conducted. The analyzed models are the milestones in the development liquid-soild two-phase flow. But the general attention is paid to the 'Growth and change model of solid particles in water-injection pipeline' (Li, Li, Wang et al., 2020). The model is a specific combination of two existing models – liquid-solid two-phase flow model (Bowen, 1980) and particle population balance model (PBM) (Hulburt & Katz, 1964).

The model describes flow of water and growth and change of solid particles in water-injection pipeline between the CUS and injection wells.

The results of studies in field application of the model are also presented. The influence of CUS outlet flowrate, temperature and initial PSD on collision probability between particles and particle growth rate of wellheads was examined (Figures 2.6-2.8). However, it is stated that the scope of the model has not been fully studied.

In the Thesis, mathematical models are observed solely for the purpose of analyzing familiarizing with existing methods. During the analysis, it was decided to continue the search for a more suitable model, which will clearly demonstrate possibility of solving problems associated with unstable flow in oil-and-gas flowline under conditions of carbon dioxide corrosion.

6.2 Results of Chapter 3

Chapter 3 is about the analysis of processes occurring in unstable flow in oil-and-gas flowline under conditions of carbon dioxide corrosion.

First of all, the real field problem was described in detail. The problem was defined – oil leaks caused by corrosion processes in the oil-and-gas flowline from well cluster-7 to OTP 'Chernovskoe' (Figure 3.1). The oilfield is operated by 'Belkamneft' named after A.A. Volkov, JSC.

The data on samples from different sections of the oil-and-gas flowline from well cluster-7 to OTP 'Chernovskoe' was presented. It includes data on sections, ruptures, corrosive tendency, fluid composition in fractions and chemical analysis of water (Tables 3.1-3.8). Factors causing and stimulating intensive corrosion processes were assumed to be: significant content of carbon dioxide in the composition of fluid and high water cut magnitudes (more than 90 wt. %).

Nevertheless, according to the data from laboratory analysis (Table 3.7), the fluid was characterized as the unstable highly-aggressive oil-in-water emulsion with solid particles and corrosion products in it and water cut of more than 90 wt. %.

Further, the analysis of software capable of simulating processes occurring during flowing of unstable highly-aggressive oil-in-water emulsion was carried out. First of all, the capabilities and principles of the dynamic multiphase flow simulator OLGA were described. OLGA simulates all sorts of hydrodynamic processes providing valuable insights through the entire production system – from reservoir pore to process facility. The simulation in OLGA is accompanied with a graphical representation of desired parameters.

Also, a special attention was paid to Multiflash simulator, which is one of external tool packages for OLGA. Multiflash allows to create many types of different fluids. A fluid can be defined in many ways – from accurate compositional or fractional analysis to very limited black oil analysis. EoS available in Multiflash, ways to define fluids, phase diagrams and fluid blending options were also analyzed and described in detail. In addition, Multiflash has the ability to perform a laboratory PVT analysis for any available fluid. The output data in Multiflash is

shown figures, plots and tables. A fluid data can be exported to a tab-file. A tab-file is a set of PVT tables of different fluid parameters in determined boundaries.

Moreover, the PIPESIM simulator was considered as the software capable of corrosion processes simulation which occur during flowing of various liquids in a pipeline. The de Waard corrosion model was highlighted as the most essential option of this simulator, providing corrosion rate calculations.

The most convenient thing is that Multiflash, OLGA and PIPESIM can be integrated into a single workspace. Thus, a fluid created in Multiflash can be used to simulate hydrodynamics in OLGA and to calculate the corrosion rate in PIPESIM.

6.3 Results of Chapter 4

Chapter 4 consists of calculations performed to simulate processes occurring in unstable highly-aggressive oil-in-water emulsion in the oil-and-gas flowline from well cluster-7 to OTP 'Chernovskoe'.

6.3.1 Multiflash

First of all, the objective was to identify production wells connected to the oil-and-gas flowline from well cluster-7 to OTP 'Chernovskoe'. As a result, 41 wells were identified (Table 4.1). Then, the data on oil and gas composition was requested from Production Department of 'Belkamneft' named after A.A. Volkov (Tables 4.3-4.4).

For analysis in Multiflash, models of oil and gas from Vereiskian-Bashkirian, Visean and Tournai oil-bearing horizons were created. The model applied to all the fluids at reservoir conditions was decided to be Peng-Robinson advanced (PRA).

After that, each fluid was saturated with water from 30 to 90 wt. %. Hence, 15 different oil-and-gas mixtures were obtained. When analyzing the phase diagrams, it was found that properties of the fluids under consideration do not differ significantly from each other (Figures 4.4-4.6).

In order to model the unstable highly-aggressive oil-in-water emulsion, it was decided to mix oil-and-gas from Vereiskian-Bashkirian, Visean and Tournai oil-bearing horizons with water cut of 90 wt. %. between each other in various proportions (Table 4.5). During the analysis of 27 oil-and-gas mixtures, it was revealed that fluids can be mixed in any proportions, as properties of the resulting fluid do not differ significantly (Figure 4.7).

For further analysis, it was decided to use one of 27 oil-and-gas mixtures, named as the Fluid-212. The reason for this is the maximum similarity of the composition to unstable

highly-aggressive oil-in-water emulsion, which is under consideration in the Thesis. The Fluid-212 was exported as a tab-file.

6.3.2 OLGA

Second of all, hydrodynamic properties of the flow were studied in OLGA. To do this, a flowpath was created in accordance with the oil-and-gas flowline from well cluster-7 to OTP 'Chernovskoe' (Figure 4.11 and Tables 4.7-4.9). Then, the Fluid-212 was imported to OLGA as a tab-file.

The hydrodynamic simulation of the Fluid-212 was performed in accordance with the data on the oil-and-gas flowline from well cluster-7 to OTP 'Chernovskoe' at Q = 3824 м^3/d during 72 hours.

The desired parameters were plotted (Figures 4.13-4.16). Analyzing results of the simulation, it was found that:

- mass flowrates – constant;
- volumetric flowrates – constant for oil and water, slightly increased for gas;
- pressure – sharp pressure gradient fluctuation (in flowline junction);
- temperature – slight temperature gradient fluctuation (in flowline junction);
- holdup – insignificant decline (in flowline junction);
- flow regime – instant transition from stratified to slug (in flowline junction);

All in all, the flow was characterized as unstable. The flowline junction in Sections 3032 and 3033 causes gas to evaporate from liquid, pressure gradient to increase and flow regime to become slug instantaneously. The flow is unstable due to instant change in flowline inner diameter from 103 mm to 147 mm.

6.3.3 PIPESIM

Finally, PIPESIM was used to simulate carbon dioxide corrosion processes by means of the de Waard corrosion model. For this, the Fluid-212 was imported to PIPESIM as a mfl-file.

For the analysis in PIPESIM, the the oil-and-gas flowline from well cluster-7 to OTP 'Chernovskoe' was divided into two separate pipelines with internal diameters of 103 and 147 mm respectively. The output data of hydrodynamic analysis in OLGA was implemented in PIPESIM as input data.

Results of corrosion rate calculation are shown in Figure 4.17 and Table 4.11:

- Sections 3033, 3035 and 3037 (internal diameter 147 mm) - corrosion rate stabilizes, more acceptable magnitudes (0.3-0.4 mm/year). Correlate with data on sample from Section 3035 (Table 3.2);
- Sections 3030 and 3032 (internal diameter 103 mm - corrosion rate is extremely high (up to 1.5 mm/year). Does not correlate with data on sample from Section 3030 (Table 3.3);

It is noteworthy that two of the four ruptures occurred in 2021 occurred exactly near the junction of Sections 3032 and 3033. (Figure 3.1).

The corrosion rate calculated in PIPESIM is not always correct:

- calculated corrosion rate in Sections 3030 and 3032 (more than 1.5 mm/year) is so due high fluid velocities, reaching 5 m/s (against 2.7 m/s in the rest of the flowline);
- the de Waard corrosion model accounts only for CO_2 corrosion, inhibitory ability of salts and negative effects caused by acids are neglected;
- the Fluid-212 has no acids, H_2S, solid particles in its composition.

Nevertheless, the de Waard corrosion model has partially fulfilled the objective during testing.

6.4 Results of Chapter 5

Chapter 5 is devoted to the laboratory study of corrosion inhibitors on the reservoir water model by means of gravimetric method. This study was carried out in order to obtain more accurate data on the corrosion rate and evaluate the index of corrosion protection of inhibitors in various media.

The reservoir water model was chosen as a corrosive medium, since it is known that the unstable and highly-aggressive water-in-oil emulsion contains more than 90% of water and a high content of CO_2. (Tables 3.2-3.5) Moreover, there is a sufficient data on chemical analysis of water (Table 5.1).

Firstly, the needed amount of salts was calculated. Then, the reservoir water model was created in accordance with data on chemical analysis of water (Table 5.1). In general, four reservoir water models of different densities of 1114, 1137, 1160, 1180 kg/m^3 were created to conduct a precise analysis.

Secondly, each reservoir water model was tested under influence of three corrosion inhibitors: SNPH-6418B, SONKOR-9020 and FLEK-IK-200. The dose of each inhibitor was 0.03 g/L. Metal samples used for the experiment are made of steel St.20, as the oil-and-gas flowline from

well cluster-7 to OTP ‘Chernovskoe’ is made of the same material. Generally, 12 experiments were carried out, which lasted more than 84 hours.

Thirdly, based on results of 12 experiments, corrosion rate was calculated for each case, as well as the index of corrosion protection (Tables 5.3-5.15). Based on it, a graphical dependence was generated (Figure 5.26). It reflects the influence of the density of the reservoir water model on the corrosion rate under carbon dioxide corrosion conditions. (Figure 5.26). It also represents the effectiveness of each corrosion inhibitor.

Based on the Figure 5.26, it was concluded that:

- corrosion rate depends on density of a corrosive medium and is not constant.
- each corrosion inhibitor has different efficiency, which depends on composition and density of a corrosive medium.
- the corrosion inhibitor SNPH-6418B has the best performance.
    a. the highest value of the index of corrosion protection of 40.91% (at ρ = 1180 kg/m^3);
    b. stable performance at all reservoir models tested;
    c. the highest magnitudes for the index of corrosion protection of 32-52%.

Moreover, corrosion rate data obtained during the laboratory experiments (Tables 5.3-5.15) correlates with the field data on corrosion rate in an uninhibited environment (Table 3.8). Thus, the main factor causing corrosion in the considered isolated system is the presence of CO_2.

Chapter 7

Conclusion

7.1 Summary

The literature review showed that the problem is extremely relevant and there is a large number of different models that describe multiphase flows. Thanks to the analysis of existing mathematical models, it was possible to make the right choice of the model in Multiflash, OLGA and PIPESIM for successful implementation of the tasks.

The analysis of processes occurring in unstable flow in oil-and-gas flowline under conditions of carbon dioxide corrosion allowed to find solutions to the problem of corrosion in the considered isolated system. Multiflash was used successfully to create a model of the considered unstable highly-aggressive oil-in-water emulsion and analyze its properties. The OLGA was implemented to make a complete hydrodynamic flow analysis. The PIPESIM simulator made it possible to calculate the corrosion rate.

Laboratory studies of corrosion inhibitors made it possible to compare experimentally calculated corrosion rates with the field tests. It approved that significant content of carbon dioxide in fluid composition and high water cut magnitudes (more than 90 wt. %) are the main factors causing corrosion in the considered isolated system. In addition, the effectiveness of each inhibitor was determined experimentally.

Methods to solve the existing problem are also proposed.

7.2 Evaluation

The Thesis considers and mathematically substantiates the unstable flow in an isolated system, which is the oil-and-gas flowline, under conditions of carbon dioxide corrosion. Also,

laboratory studies of corrosion inhibitors were carried out on various reservoir water models with determination of their effectiveness.

7.3 Future Work

In order to solve the problem of corrosion, the following solutions can be applied:

- evaluation of the economic benefit of each corrosion inhibitor;
- performing field tests of the corrosion inhibitor SNPH-6418B and compare its effectiveness with the effectiveness of the corrosion inhibitor RIK-1 (58.7%), which is currently used in 'Belkamneft' named after A.A. Volkov, JSC;
- analyze the combined effect of two corrosion inhibitors in order to obtain the best synergistic effect;
- construction of a new oil-and-gas flowline with an internal diameter of 147 mm instead of the existing oil-and-gas flowline with an internal diameter of 103 mm (Sections 3030 and 3032). The goal is to eliminate the zone that causes flow instability and get rid of high fluid velocities in the system;
- construction of a completely new oil-and-gas flowline with anti-corrosion coating;
- construction of the PWRU (preliminary water removal unit) at the junction of Sections 3032 and 3033 of the existing oil-and-gas flowline from well cluster-7 to OTP 'Chernovskoe'. The goal is to remove excessive water from the flow.

However, the cost-effectiveness analysis must be done for each suggested solution of the problem of corrosion in order to be successfully applied in field conditions.

References

Abegg, C.F., Stevens, J.D., & Larson, M.A. (1968). Crystal size distributions in continuous crystallizers when growth rate is size dependent. *AIChE Journal*. https://doi.org/10.1002/aic.690140121

Bowen, R. (1980). Incompressible porous media models by use of the theory of mixtures. *International Journal of Engineering Science*. https://doi.org/10.1016/0020-7225(80)90114-7

Crowe, C., Sharma, M., & Stock, D. (1977). The Particle-Source-In Cell (PSI-Cell) Model for Gas-Droplet Flows. *Journal of Fluids Engineering*. https://doi.org/10.1115/1.3448756

de Waard, C., Lotz, U., and Dugstad, A. (1995). Influence of Liquid Flow Velocity on CO_2 Corrosion: A Semi-Empirical Model. *In CORROSION 95. Orlando, Florida: NACE International.*

El-Dessouky, H. & Ettouney, H. (2002). Fundamentals of Salt Water Desalination. *Amsterdam, Elsevier.*

Fan, R., Marchisio, D., & Fox, R. (2004). Application of the direct quadrature method of moments to polydisperse gas-solid fluidized beds. *Powder Technology*. https://doi.org/10.1016/j.powtec.2003.10.005

GOST 9.905-82. (1983). ГОСТ 9.905-82. Методы коррозионных испытаний. Общие требования. *[Unified system of corrosion and ageing protection. Corrosion test methods. General requirements]*.

GOST 9.502-82. (1984). ГОСТ 9.502-82. Ингибиторы коррозии металлов для водных систем. Методы коррозионных испытаний. *[Unified system of corrosion and ageing protection. Inhibitors of metals corrosion for aqueous systems. Methods of corrosion tests]*.

GOST 9.506-87. (1988). ГОСТ 9.506-87. Ингибиторы коррозии металлов в водно-нефтяных средах. Методы определения защитной способности. *[Unified system of corrosion and ageing protection. Corrosion inhibitors of metals in water-petroleum media. Methods of protective ability evaluation]*.

Ho, C.A. & Sommerfeld, M. (2002). Modelling of micro-particle agglomeration in turbulent flows. *Chemical Engineering Science.* https://doi.org/10.1016/S0009-2509(02)00172-0

Hulburt, H. & Katz, S. (1964). Some problems in particle technology: A statistical mechanical formulation. *Chemical Engineering Science.* https://doi.org/10.1016/0009-2509(64)85047-8

Infochem/KBC Advanced Technologies Ltd. (2015). *User Guide for Multiflash for Windows.*

Kunz, O., Klimeck, R., Wagner, W., Jaeschke, M. (2007). The GERG-2004 wide-range equation of state for natural gases and other mixtures. *GERG Technical Monograph 15.*

Leporini, M., Terenzi, A., Marchetti, B. et al. (2019). Experiences in numerical simulation of wax deposition in oil and multiphase pipelines Theory versus reality. *Journal of Petroleum Science and Engineering.* https://doi.org/10.1016/j.petrol.2018.11.087

Lewis, A., Seckler, M., Kramer, H. et al. (2015). Industrial Crystallization: Fundamentals and Applications. *UK, Cambridge University Press.* https://doi.org/10.1017/CBO9781107280427

Li, G., Li, C., Wang, J., et al. (2020). Study on Growth and Change of Solid Particles with Water Flow in Oilfield Water-Injection Pipeline. *Tehnicki Vjesnik-technical Gazette*. https://doi.org/10.17559/TV-20191129074559

Markin A.N., Nizamov R.E., Sukhoverkhov S.V. (2011). Нефтепромысловая химия: практическое руководство. *Владивосток: Дальнаука. [Production Chemistry: guidance manual. Vladivostok: Dalnauka]*.

Pack, D.J., Parks, D.W., & Chesnoy, A.B. (2012). Gas pipeline preferential site selection occurrence for elemental sulphur & other particle matter formation & deposition. *Journal of Petroleum Science and Engineering.* https://doi.org/10.1016/j.petrol.2012.06.022

Park, S. & Lee, K. (2002). Analytical solution to change in size distribution of polydisperse particles in closed chamber due to diffusion and sedimentation. *Atmospheric Environment.* https://doi.org/10.1016/S1352-2310(02)00673-8

Pope, S. (1980). Probability distributions of scalars in turbulent shear flow. Symposium on Turbulent Shear Flows. *Massachusetts Institute of Technology.*

Riazi, M.R., Daubert, T.E. (1986). Analytical Correlations Interconvert Distillation Curve Types. *Oil & Gas Journal.*

RNK, UNPP NIPIneft (2016). Дополнение к технологической схеме разработки Черновского нефтяного месторождения Удмуртской Республики. Книга 1. Текстовая часть. *[Addition to the technological scheme for the development of the Chernovskoye oilfield in the Udmurt Republic. Book 1. Text part]*.

RNK, UNPP NIPIneft (2016). Дополнение к технологической схеме разработки Черновского нефтяного месторождения Удмуртской Республики. Книга 2. Текстовая часть. *[Addition to the technological scheme for the development of the Chernovskoye oilfield in the Udmurt Republic. Book 2. Text part]*.

Robinson, D.B. and Peng, D.Y. (1976). A New Two-Constant Equation of State Industrial and Engineering Chemistry: Fundamentals. *Industrial & Engineering Chemistry Fundamentals*. http://dx.doi.org/10.1021/i160057a011

Schlumberger Software (2021). *OLGA Dynamic Multiphase Flow Simulator.*

Schlumberger Software (2021). *PIPESIM Flow Modeling.*

Song, G., Li, Y., Wang, W. et al. (2018). Numerical simulation of pipeline hydrate particle agglomeration based on population balance theory. *Journal of Natural Gas Science and Engineering*. https://doi.org/10.1016/j.jngse.2018.01.009

Soo, S. (1989). Particulates and Continuum-Multiphase Fluid Dynamics: Multiphase Fluid Dynamics. *New York: CRC Press.* https://doi.org/10.1201/9780203744291

Spalding, D.B. (1972). Mathematical Models of Continuous Combustion. *New York: Springer.* https://doi.org/10.1007/978-1-4684-1998-6_1

Starling, K.E. (1973). Fluid Thermodynamic Properties for Light Petroleum Systems. *Houston, Gulf Publishing Co.*

Sun, L., Ely, J.F. (2005). A corresponding states model for generalized engineering equations of state. *International Journal of Thermophysics.*

Tchen, C. (1947). Mean value and correlation problems connected with the motion of small particles suspended in a turbulent fluid. *Netherlands: Delft University.*

VNIISPTneft (1987). РД 39-0147103-362-86. Руководящий документ. Руководство по применению антикоррозионных мероприятий при составлении проектов обустройства и реконструкции объектов нефтяных месторождений. *[RD 39-0147103-362-86. Normative*

document. Normative on the application of anti-corrosion measures in the preparation of projects for the development and reconstruction of oil fields].

Wang, K., Yu, S., & Peng, W. (2019). A novel moment method using the log skew normal distribution for particle coagulation. *Journal of Aerosol Science*. https://doi.org/10.1016/j.jaerosci.2019.04.013

List of Figures

List of Tables

Nomenclature

A	surface area of a metal sample	[m^2]
A_l	parameter of liquid phase	
Cc	multiplier to correct for inhibitor efficiency or match to field data	
C_p	heat capacity at constant pressure	[J/(mol·K)]
C_v	heat capacity at constant volume	[J/(mol·K)]
d	pipe diameter	[m]
D_x	diffusion coefficient	
fCO_2	fugacity of CO_2	[atm]
Fs	scaling factor	
Fg	glycol reduction effect	
G_0	growth rate of the crystal nucleus	[m/s]
L	length	[m]
L_p	particle size	[m]
$M(X_xY_y)$	molecular weight of the mixture X_xY_y	
$M(X)$	molecular weight of the element X	
$M(Y)$	molecular weight of the element Y	
M_{comp}	molecular weight of a component	
M_{salt}	molecular weight of a salt	
m_{comp}	mass of a component per 1 liter of a solution	[g/L]
m_{inh}	mass of a corrosion inhibitor per 1 liter of a solution	[g/L]
m_{salt}	mass of a salt per 1 liter of a solution	[g/L]
m_1	mass of a metal sample before the experiment	[g]
m_2	mass of a metal sample after the experiment	[g]
nCO_2	mole fraction of CO_2	
$n(v, x, t)$	particle number density function	[a/m^3]

P	pressure	[Pa]
pCO_2	partial pressure of CO_2	[atm]
P_{total}	total pressure	[atm]
pH_{act}	actual pH of the system	
pH_{CO2}	pH of dissolved CO_2 in pure water	
Q	volumetric flowrate	[m^3/d]
Q_m	mass flowrate	[kg/s]
Q_x	energy transfer source term	[J]
$S(v, x, t)$	kernel function of dynamic events of particles	
T	temperature	[K]
Ts	corrosion rate inversion temperature	[K]
t	duration of the experiment	[h]
U_L	liquid velocity	[m/s]
V	average rate of the v particle in the i direction	[m/s]
V_{cor}	corrosion rate	[mm/year]
V_C	corrosion rate	[g/(m^2·h)]
V_{CP}	corrosion rate (penetration)	[mm/year]
V_{Co}	corrosion rate without inhibitor	[mm/year]
V_{Ci}	corrosion rate with an inhibitor injected	[mm/year]
V_m	mass transfer rate term	[mm/year]
V_r	reaction rate term	[mm/year]
v_l	velocity of liquid phase	[m/s]
w_{inh}	amount of a corrosion inhibitor to be injected	[µL]
w_{fluid}	volume of a solution	[L]
WC	water cut	[wt. %]
x	number of molecules of the element X	

y	number of molecules of the element Y	
Z	index of corrosion protection	[%]

Greek symbols:

ρ	density	[kg/m^3]
ρ_{inh}	density of a corrosion inhibitor	[g/m^3]
ρ_l	density of liquid phase	[kg/m^3]

Abbreviations

AGMU	automated group measuring unit
API	American Petroleum Institute
BIP	binary interaction parameter
CIS	chemical injection skid
CSP	corresponding-states principle
CUS	center united station
DEG	diethylene glycol
EoS	equation of state
GERG	Geochemical and Environmental Research Group
GOR	gas-oil ratio
GUI	graphical user interface
LNG	liquefied natural gas
MEG	methyl ethylene glycol
MPS	multiphase pump station
OTP	oil treatment plant
PBM	particle population balance model
PR	Peng-Robinson
PRA	Peng-Robinson advanced
PSD	particle size distribution
PVT	pressure, volume, temperature
PWRU	preliminary water removal unit
SARA	Saturate, Aromatic, Resin and Asphaltene
SCN	single carbon number
STO	stock tank oil
TBP	true boiling point
TEG	triethylene glycol

VLE	vapour-liquid equilibria